Politecnico di Torino

DEPARTMENT OF MECHANICAL AND AEROSPACE ENGINEERING (DIMEAS)

Master of Science in Mechanical Engineering

2024/2025

Data-based Nonlinear Modeling of Hysteretic Systems: Application to Stockbridge Dampers

Master's Thesis

July 2025

Mohammad Reza Abedi

Supervisors:

Prof. Dario Anastasio

Prof. Stefano Marchesiello

Abstract

Stockbridge dampers are widely used in overhead transmission lines to mitigate aeolian vibrations and protect conductors from fatigue failure. This research addresses the limitations of linear damping models in accurately representing the dynamic behavior of Stockbridge dampers, utilizing Bouc-Wen non-linear damping, and captures experimentally observed vibrations. A novel approach is proposed to develop a nonlinear model of Stockbridge dampers using neural networks to learn complex nonlinear relationships and genetic algorithms for parameter optimization. The objectives of this research are to improve the accuracy of damper performance prediction, enhance design optimization strategies, and gain deeper insights into the damper's complex dynamics. The methodology involves analyzing similar SDOF and MDOF systems and exercising nonlinear properties, and applying optimization to validate the approach, developing a neural network model that accounts for nonlinearities and 3D motion, validated against experimental data and finite element analysis results. Genetic algorithms will be used to optimize model parameters and explore potential improvements in damper design. The expected outcomes of this research include a more accurate and reliable tool for analyzing and designing Stockbridge dampers, resulting in enhanced vibration mitigation in slender structures, such as overhead power lines and cable-stay bridges.

Acknowledgments

I would like to express my sincere gratitude to my thesis supervisor, Prof. Dario Anastasio, for his invaluable guidance, support, and continuous encouragement throughout the duration of this project. His expertise and constructive feedback greatly enriched my research and significantly contributed to my professional and personal growth.

Special thanks go to Prof. Stefano Marchesiello for his critical support and valuable insights throughout the project.

Lastly, I extend my appreciation to Politecnico di Torino and Dynamics and Identification Research Group for providing the resources and facilities essential for conducting this research.

Contents

List of Figures

List of Tables

List of Acronyms

NN	Neural Network
FFNN	Feedforward Neural Networks
RNN	Recurrent Neural Networks
LSTM	Long Short-Term Memory
CNN	Convolutional Neural Networks
PINN	Physics-Informed Neural Network
GA	Genetics Algorithm
FEA	Finite Element Analysis
NNO	Neural Network Optimization
ANN	Artificial Neural Network
SDOF	Single Degree of Freedom
2DOF	Two Degree of Freedom
PSD	Power Spectral Density
DOF	Degree of Freedom
BW	Bouc-Wen
FEM	Finite Element Model

1 Introduction

Stockbridge dampers play a crucial role in mitigating wind-induced vibrations on slender structures such as overhead power lines and cable-stay bridges. These vibrations, particularly aeolian vibrations, can lead to fatigue failure in conductors, thereby necessitating effective damping solutions to ensure the longevity and reliability of these critical infrastructures. The Stockbridge damper has been widely adopted across various cable-supported structures for its ability to dissipate energy and reduce vibration amplitudes. Aeolian vibration, a significant concern for overhead lines, occurs primarily in the vertical plane due to alternating vortex shedding caused by wind flow. This type of vibration is a principal cause of failure in conductor strands, making the effective application of Stockbridge dampers essential. Since their invention in the 1920s, Stockbridge dampers have remained a relevant and effective solution for controlling these vibrations[1], [2].

Aeolian vibration is a specific type of wind-induced oscillation that affects cylindrical structures such as overhead power line conductors. This phenomenon arises from the flow of wind across the conductor, which disrupts the airflow and causes the alternating shedding of vortices on the leeward (downwind) side. These shed vortices, known as Karman vortices, create fluctuating pressure zones around the conductor, resulting in periodic forces that induce vibration. Typically, aeolian vibrations are characterized by high frequencies, ranging from 3 to 50 Hertz with a wind speed of 1-7 m/s, and small amplitudes, measured in millimeters to centimeters[3]. The frequency of these vibrations is directly related to the wind speed and inversely proportional to the diameter of the conductor, a relationship that can be approximated by the Strouhal formula: $f = St * V/D$, where 'f' is the frequency, 'St' is the Strouhal number (an empirical constant), 'V' is the wind speed, and 'D' is the conductor diameter. This formula reveals that for a given wind speed, conductors with smaller diameters are more prone to experiencing higher frequency vibrations compared to larger conductors[2], [4].

Aeolian vibrations pose a significant concern for the structural integrity of overhead power lines. The continuous, high-frequency oscillations induce repetitive bending stresses in the conductor strands, particularly at support points where the conductor is clamped to towers and insulators. Over time, these cyclic stresses can lead to fatigue failure of the conductor strands, which can compromise the mechanical strength and electrical conductivity of the power line. Additionally, aeolian vibrations can cause wear and tear on insulators and other hardware components, potentially leading to electrical faults and increased maintenance costs[3].

1.1 Limitations of Linear Damping Models for Stockbridge Dampers

Linear viscous damping models, which typically assume that the damping force is directly proportional to the velocity of the vibrating object, often prove inadequate in accurately representing the behavior of Stockbridge dampers. The dynamic behavior of Stockbridge dampers involves several sources of nonlinearity that deviate significantly from this linear assumption. While linear models may provide acceptable results in some cases, they often fall short, particularly those involving complex interactions within a Stockbridge damper. Simplified linear models, such as mass-spring-viscous damper systems, have been shown to yield poor results when predicting the forced response of these devices[5].

One of the primary sources of nonlinearity in Stockbridge dampers is the friction that occurs between the individual strands of the messenger cable. This friction, which is the principal

mechanism through which the damper dissipates energy, exhibits nonlinear characteristics. These characteristics include stick-slip behavior, where the friction force changes abruptly depending on whether the surfaces are sliding or stuck, and a dependence on the amplitude of vibration. It has been noted that the high efficiency of Stockbridge dampers can be attributed to this nonlinear behavior. To better represent this, more complex models incorporating distributed Jenkin elements, which consist of linear springs and Coulomb friction elements arranged in parallel, have been used. The dynamic response of Stockbridge dampers is indeed markedly nonlinear and hysteretic due to this frictional dissipation of energy localized on the contact surfaces between adjacent wires of the messenger cable[5], [6].

Geometric nonlinearities also play a significant role in the behavior of Stockbridge dampers. During vibration, the messenger cable undergoes large deflections and stretching, which introduce nonlinearities in its stiffness[5], [6]. The relationship between the applied force and the resulting deformation becomes non-proportional, especially at larger vibration amplitudes. This geometric elongation and the resulting nonlinear stiffness are crucial aspects that linear models often neglect. Furthermore, the bending stiffness of the messenger cable might not be uniform along its length, exhibiting a "boundary layer like transition" in the end zones, which significantly affects the overall behavior of the damper.

Material nonlinearities can also contribute to the complex dynamics of Stockbridge dampers. The messenger cable, being a stranded structure, and the materials used in its construction may exhibit nonlinear material properties under dynamic loading conditions. Experimental data has shown that parameters like flexural stiffness and the loss factor of the messenger cable are not constant but depend on the frequency of excitation, indicating nonlinear material behavior[6].

The use of linear models can lead to several inaccuracies in predicting the performance of Stockbridge dampers. These models may fail to accurately predict the resonant frequencies of the damper, which are critical for its effectiveness. They may also provide incorrect damping ratios, leading to an overestimation or underestimation of the damper's ability to dissipate energy. The overall effectiveness of the damper across a range of vibration amplitudes and frequencies is also poorly captured by linear representations. Experimental observations have revealed a strong nonlinear behavior, where the natural frequencies and impedance curves of the damper vary significantly with the amplitude of the excitation[2], [6]. Linear analytical models have been acknowledged as insufficient to fully understand the response of transmission line conductors in the presence of Stockbridge dampers. Comparisons between linear analytical models and experimental results have shown that the mode frequencies predicted by linear models can be significantly lower than those observed experimentally and do not reflect the dependence on the driving velocity, highlighting the shortcomings of such approaches. Several research efforts have specifically addressed these limitations, advocating for the development and application of nonlinear models to better predict the dynamic response of Stockbridge dampers.

1.2 Neural Network Modelling of Nonlinear Dynamic Systems

Neural networks (NNs) have emerged as powerful and versatile tools for modeling complex nonlinear relationships in various engineering disciplines, including the analysis of dynamic systems. Their inherent ability to learn intricate patterns directly from data makes them particularly well-suited for capturing the nonlinear behavior often exhibited by real-world systems, where traditional linear models may prove inadequate. The strength of NNs lies in

their capacity to approximate complex nonlinear mappings and adapt to the nonlinearities present in the behavior patterns of a system[7], [8], [9], [10].

One of the key advantages of neural networks is their ability to capture nonlinear behavior that traditional linear models often fail to represent. For instance, in Stockbridge dampers, damping and stiffness characteristics are not constant but can vary significantly with the amplitude of vibration. Linear models, with their fixed parameters, cannot account for such amplitude-dependent behavior. However, neural networks can be trained to learn these complex relationships from experimental or high-fidelity simulation data, providing a more accurate representation of the system's dynamics. Studies have shown that parameters like the natural frequency and flexural stiffness of a Stockbridge damper can depend on the amplitude of the base excitation, a nonlinearity that can be effectively modeled using techniques like the Bouc-Wen hysteretic model, which can be implemented within a neural network framework.

Various types of neural network architectures are suitable for modeling dynamic systems, each with its own strengths and applications. Feedforward neural networks (FFNNs) are a fundamental type capable of learning complex mappings between inputs and outputs. Recurrent neural networks (RNNs), particularly their variants like Long Short-Term Memory (LSTM) networks, are designed to process sequential data and can capture temporal dependencies in dynamic systems, making them suitable for modeling time-varying behavior. Convolutional neural networks (CNNs), while initially developed for image processing, can also be adapted for dynamic system modeling, especially when dealing with multi-dimensional data or when feature extraction from time-series is required. The choice of the appropriate neural network architecture often depends on the specific characteristics of the dynamic system being modeled and the nature of the available data[9].

The application of neural networks in the context of vibration damping has garnered increasing attention. Researchers have explored using NNs for nonlinear modal identification in dynamical systems, aiming to extract nonlinear normal modes that provide a comprehensive representation of the system's dynamics. Physics-informed neural networks (PINNs) represent a particularly promising approach, where known physical laws, such as the governing differential equations of motion, are incorporated into the neural network's training process[9]. This integration of physics can improve the accuracy and generalization capabilities of the models, especially for nonlinear structural systems where damping is a crucial factor. Deep learning techniques, including neural networks, are also being used to generate reduced-order models of complex systems, including vibratory systems, for efficient simulation and optimization.

Neural networks offer several advantages for modeling dynamic systems. Their ability to learn complex patterns from data allows them to capture intricate nonlinearities that might be difficult to model using traditional analytical methods. They can also handle noisy data to some extent and have the potential to generalize to unseen conditions, making the trained models useful for prediction and analysis beyond the specific data they were trained on. The data-driven nature of neural networks enables them to model system behavior directly from observed data, without requiring explicit knowledge of the underlying physical equations in all cases.

1.3 Genetic Algorithms for Optimization in Structural Dynamics

Genetic algorithms (GAs) are powerful stochastic optimization techniques inspired by the principles of natural selection and genetics. These algorithms have proven to be highly effective in solving complex optimization problems across various engineering domains, including structural dynamics. GAs work by maintaining a population of potential solutions, which are iteratively improved through processes analogous to natural selection, crossover, and mutation, ultimately converging towards an optimal or near-optimal solution[11].

In the context of Stockbridge dampers, genetic algorithms can be effectively utilized to optimize various design parameters to enhance their vibration damping performance. These parameters can include the mass distribution of the damper weights, the length and material properties of the messenger cable, and even the overall geometry of the damper. The objective of such optimization can be to maximize the attenuation of vibrations in the conductor, minimize the cost of the damper materials, or achieve a balance between multiple performance criteria. For example, studies have proposed using GAs to find the optimal parameters that lead to maximum vibration reduction across the expected range of wind-induced frequencies. The mass of the damper weights and the length of the messenger cable have been identified as key variables influencing vibration attenuation, making them suitable parameters for optimization using GAs. Furthermore, GAs have been applied to the design of asymmetric Stockbridge dampers to improve their efficiency in mitigating wind-induced vibrations by optimizing their multiple resonance frequencies[12].

Genetic algorithms offer several advantages that make them well-suited for optimization problems in structural dynamics. They can effectively handle complex and discontinuous design spaces, which are often encountered in structural optimization. Unlike gradient-based methods, GAs do not require gradient information of the objective function, making them applicable to a wider range of problems, including those where the objective function is not smooth or differentiable. Their population-based search strategy increases the likelihood of finding globally optimal or near-optimal solutions, rather than getting stuck in local optima.

The integration of genetic algorithms with other computational methods, such as finite element analysis (FEA) and neural networks, has proven to be particularly powerful for tackling complex engineering problems. For example, GAs can be used to find the optimal set of design parameters that are then evaluated using a detailed FEA model. Similarly, GAs can be employed to optimize the architecture and training parameters of neural networks for specific applications. These hybrid approaches leverage the strengths of each method, resulting in more effective optimization and model identification strategies.

1.4 Scope and contributions

1.4.1 Use of nonlinear damping model; Bouc-Wen model in Stockbridge dampers

This thesis addresses the limitations of linear simulation models for Stockbridge dampers by introducing a novel nonlinear modeling approach based on the Bouc-Wen model. Traditional linear models often fall short in accurately capturing key dynamic behaviors of these dampers, such as the softening and hardening responses observed under varying excitation amplitudes. Additionally, they tend to exhibit significant inaccuracies near the system's natural frequencies and in the lower frequency range, where nonlinear effects become more pronounced. By incorporating the Bouc-Wen model—a widely used framework for representing hysteretic

nonlinearities—we aim to overcome these shortcomings and provide a more realistic and predictive simulation of the damper's dynamic response. This approach enables a better understanding of the energy dissipation mechanisms and contributes to more accurate design and analysis of vibration mitigation systems in overhead power lines.

1.4.2 Formulation of a NN-based parameter estimator for Bouc-Wen nonlinearities

Replacing traditional Genetic Algorithm (GA) optimization with Neural Network Optimization (NNO) results in more accurate and efficient optimization outcomes. NNO acts as a surrogate model that integrates an Artificial Neural Network (ANN) with a Genetic Algorithm, combining the strengths of both approaches. The ANN is trained to approximate the objective function, allowing the optimizer to explore the design space much faster than evaluating the full model at every iteration. This hybrid approach addresses several common issues associated with standalone GA methods, such as long computation times, a high chance of becoming trapped in local optima, and convergence instability. By using the ANN as a predictive model, the NNO guides the search process more intelligently, significantly reducing the number of expensive function evaluations while improving the likelihood of finding a global optimum. This makes it especially valuable for complex, computationally intensive engineering problems like those encountered in modeling and optimizing Stockbridge dampers.

2 Literature Review

The mitigation of unwanted vibrations is a critical aspect of mechanical and structural engineering, ensuring the stability, safety, and extended lifespan of a wide array of systems. From intricate machinery to expansive infrastructure, the demand for effective damping solutions has grown in tandem with advancements in technology and construction. This literature review aims to provide a comprehensive exploration of the evolution of damping devices, the conventional design methodologies employed for various types of dampers, a focused examination of Stockbridge dampers utilized in overhead power lines, and an in-depth analysis of nonlinear hysteresis models, with particular attention to the Bouc-Wen model and its extensions, as well as the application of cubic stiffness elements in representing nonlinear structural behavior.

2.1 Stockbridge Dampers

The Stockbridge damper, a specific type of tuned mass damper, was invented in the 1920s by George H. Stockbridge, an engineer working for Southern California Edison. Its invention was a direct response to the problem of fatigue failures observed in overhead transmission lines caused by wind-induced vibrations, particularly Aeolian vibrations. Over the years, the basic design of the Stockbridge damper has undergone several evolutions to enhance its efficiency and broaden the range of vibration frequencies it can effectively address. Early Stockbridge dampers were considered "2-Response" designs, featuring equal weights and messenger cable lengths, which resulted in two primary resonant frequencies. Modern designs have largely replaced the original concrete blocks with metal bell-shaped weights, often hollow, with the damper cable fixed internally to the distal end to allow for relative motion. A significant advancement was the development of asymmetric Stockbridge dampers, also known as 4-R dampers, which utilize unequal weights and messenger cable lengths to generate four distinct resonant frequencies[4]. This increased number of resonant frequencies provides more comprehensive coverage across the spectrum of Aeolian vibration frequencies, improving the damper's overall effectiveness.

Stockbridge dampers function as tuned mass dampers specifically engineered to suppress Aeolian vibrations, which are high-frequency, low-amplitude oscillations that occur in overhead power lines due to wind passing over the conductors. These vibrations, if left unchecked, can lead to damaging stress fatigue in the conductor strands, ultimately causing failure. The design of a Stockbridge damper involves several key parameters that are carefully considered to ensure effective vibration mitigation. The mass of the weights, often referred to as hammerheads, significantly influences the damper's resonant frequencies and its capacity to dissipate energy. Modern Stockbridge dampers frequently employ unequal weights to achieve multiple resonant frequencies, thereby broadening the range of vibrations that can be effectively damped. The length of the messenger cable, the flexible steel strand connecting the weights to the central clamp, determines the stiffness of the damper and consequently its resonant frequencies. Asymmetric dampers are characterized by unequal lengths of the messenger cable on either side of the clamp. The material properties of the messenger cable are also crucial, with steel being the standard choice, often in a specific strand configuration like 19-strand, which enhances inter-strand friction and thus the energy dissipation capability of the damper. The clamp is designed to securely attach the damper to the conductor, ensuring efficient transfer of vibration energy from the power line to the damper. Tuning is a critical

aspect of Stockbridge damper design, involving the careful selection of the mass of the weights and the length of the messenger cable to match the mechanical impedance of the damper to that of the specific power line being protected, across the relevant frequency range of Aeolian vibrations (typically 3 to 150 Hz). In some cases, a degree of detuning, where the damper's natural frequency is intentionally slightly different from the cable's, is employed to maintain effectiveness under varying cable tension forces caused by temperature changes and loads. In the application of Stockbridge dampers to overhead power lines, their placement is typically at anti-nodes, which are points of maximum displacement along the vibrating conductor, located near the suspension clamps[4]. Often, two dampers are installed per span, though longer spans may require more.

Several authors have examined the dynamics of the Stockbridge damper. The common approach is to experimentally determine its impedance curve[13], [14], [15], [16]. Another approach is to model the Stockbridge damper as a two degree-of-freedom system[1], [17].

An attempt to depart from the conventional way of modeling the Stockbridge damper was reported in Refs. [18], [19]. The messenger cable was modeled as an Euler–Bernoulli beam and the counterweight was modeled as mass with a rotatory inertia. Both studies omitted the geometric nonlinearity of the messenger cable and employed the finite element method.

The current study presents an analytical model that accounts for the nonlinearity of the messenger cable. Numerous authors (see Refs. [20], [21], [22], [23], [24]) have examined the nonlinear vibration of beams with attached mass or spring mass. However, these investigations are limited to cases with end support.

2.2 Nonlinear Hysteresis Models

While linear viscous damping models have historically been prevalent in engineering analysis due to their mathematical simplicity, they often fall short in accurately representing the energy dissipation mechanisms in many real-world systems, particularly when subjected to higher levels of excitation or when dealing with materials exhibiting complex behaviors. These linear models may lead to inaccurate predictions, either underestimating or overestimating peak responses, miscalculating transient behaviors, and failing to capture unique characteristics present in actual systems. Many real-world systems exhibit damping that is not constant but rather depends on the amplitude and frequency of vibration, aspects that linear models with fixed damping coefficients cannot adequately address. This necessitates the use of more sophisticated nonlinear models to accurately predict and analyze the dynamic behavior of such systems. Hysteresis, a phenomenon characterized by a memory-dependent, multi-valued relationship between force and deformation, plays a crucial role in the damping of many materials and devices. In hysteretic damping, the restoring force not only depends on the instantaneous deformation but also on the history of that deformation. This type of damping often arises from internal friction within materials during cyclic loading, resulting in a phase lag between the applied stress and the resulting strain, and a dissipation of energy over each cycle of vibration. To accurately represent the intricate shapes of hysteresis loops observed in various damping devices and materials, including phenomena like softening, hardening, and pinching, nonlinear hysteresis models are essential. These models provide a more realistic depiction of the energy dissipation processes in systems where linear damping assumptions are no longer valid.

The Bouc-Wen model stands as a prominent nonlinear hysteretic model, first introduced by Robert Bouc in 1967 and later generalized by Yi-Kwei Wen in 1976[25]. This model has gained significant popularity due to its versatility in analytically capturing a wide range of hysteretic patterns and its mathematical tractability, allowing for smooth transitions between elastic and post-elastic behaviors. The Bouc-Wen model and its subsequent variants and extensions have found extensive applications in structural control, particularly in modeling the behavior of magneto-rheological dampers, base-isolation devices used in buildings, and various other types of damping devices. The mathematical formulation of the Bouc-Wen model often expresses the restoring force of a single-degree-of-freedom system as a combination of a linear elastic component and a nonlinear hysteretic component. The hysteretic component, denoted by the variable z, is governed by a first-order nonlinear differential equation that captures the memory-dependent nature of hysteresis. A common form of this equation is ($\dot{z} = A\,\dot{x} - \beta|\dot{x}||z|^{\nu-1}\,z - \gamma\,\dot{x}|z|^{\nu}$), although variations exist with slightly different parameterizations[25], [26]. Several key parameters within the Bouc-Wen model dictate the shape and characteristics of the resulting hysteresis loop. Parameter A controls the amplitude or scale of the hysteresis loop and is often normalized to 1 to eliminate redundancy in the parameter set. The parameters β and γ primarily govern the shape and geometry of the hysteresis loop, including the transition between elastic and plastic behavior regimes. Their ratio influences the degree of hardening or softening exhibited by the system. To ensure uniqueness of the parameters, a constraint such as ($\beta + \gamma = 1$) is often imposed. The positive exponent "n" controls the smoothness of the transition from the elastic to the post-elastic region of the hysteresis loop. Higher values of n result in a more abrupt transition, approximating the bilinear behavior often seen in plasticity models. Another parameter, α, often appears in the equation for the restoring force and represents the ratio of the post-yield stiffness to the pre-yield stiffness of the system[25], [26], [27].

In nonlinear structural behavior, cubic stiffness elements play a significant role in modeling systems where the stiffness is not constant but varies with the amplitude of deformation. In contrast to the linear relationship between restoring force and displacement ($F = k\,x$), a cubic stiffness element introduces a term proportional to the cube of the displacement (k_3x^3), resulting in a nonlinear restoring force equation: ($F = k_1x + k_3x^3$). This type of nonlinearity is often employed to represent geometric nonlinearities, particularly the stiffening effect observed in structural elements like beams and plates undergoing large deflections due to in-plane stretching of their mid-surfaces. The presence of cubic stiffness can lead to the phenomenon of amplitude-dependent natural frequencies, where the frequency of vibration changes as the amplitude of motion varies. Systems incorporating cubic stiffness may also exhibit jump resonance, characterized by sudden changes in vibration amplitude as the excitation frequency is swept through the system's natural frequency range. The sign of the cubic stiffness coefficient k_3 determines whether the system exhibits hardening or softening spring behavior. A positive value $k_3 > 0$ indicates a hardening spring, where the restoring force increases more rapidly than in a linear spring at larger displacements, leading to an increase in effective stiffness and typically causing the resonance peak in the frequency response to bend towards higher frequencies. Conversely, a negative value $k_3 < 0$ signifies a softening spring, where the restoring force increases less rapidly with displacement, resulting in a decrease in effective stiffness at larger amplitudes and causing the resonance peak to bend towards lower frequencies. The nonlinear behavior introduced by cubic stiffness elements can significantly interact with the damping mechanisms present in the system. The amplitude-dependent

frequency can shift the system's resonance relative to the excitation frequency, thereby influencing the level of vibration and the amount of energy dissipated by any dampers present. In systems where cubic stiffness is significant, linear viscous damping models may not be adequate to accurately represent the energy dissipation. Instead, nonlinear damping models, which may include terms proportional to higher powers of velocity (e.g., cubic damping), might be necessary to capture the complex interplay between the nonlinear stiffness and damping forces. Therefore, cubic stiffness elements are essential for accurately modeling the nonlinear dynamic behavior of many structural and mechanical systems, particularly those experiencing large deformations or exhibiting hardening or softening spring characteristics and understanding their interaction with damping is crucial for designing effective vibration control strategies.

3 Neural Network Optimization: A Surrogate-Based Approach

3.1 Introduction

Optimization problems are fundamental across a vast spectrum of scientific and engineering disciplines, ranging from designing efficient algorithms to developing novel materials and controlling complex systems. While numerous traditional optimization methods exist, a significant challenge arises when dealing with objective functions that are computationally expensive to evaluate, particularly in the context of nonlinear least-squares problems. The increasing complexity of models and simulations in various fields often leads to objective functions where a single evaluation can consume substantial computational resources, rendering direct optimization via traditional methods impractical due to the prohibitive number of evaluations required for convergence. Nonlinear least-squares problems, which aim to minimize the sum of squared differences between observed and predicted values, are prevalent in areas such as data fitting, parameter estimation, and model calibration. These problems are inherently nonlinear and can possess intricate landscapes with multiple local minima, further complicating the optimization process. Traditional optimization algorithms, especially those relying on gradient information, can struggle with such complexities and the associated high computational costs. To address these limitations, more advanced techniques have emerged, one of the most promising being Neural Network Optimization (NNO). NNO represents a surrogate-based approach that leverages the power of Artificial Neural Networks (ANNs) and optimization algorithms, such as Genetic Algorithms (GAs), to efficiently tackle these challenging optimization problems. This report aims to provide a detailed explanation of the NNO technique, elucidating its underlying principles, step-by-step process, advantages, limitations, and potential applications across various domains.

3.2 Fundamentals of Neural Network Optimization (NNO)

The Neural Network Optimization (NNO) algorithm offers a strategy for solving complex optimization problems, especially nonlinear least-squares problems, where evaluating the objective function is computationally demanding. At its core, NNO employs an Artificial Neural Network (ANN) as a surrogate model, effectively a computationally cheaper stand-in, to approximate the behavior of the expensive objective function (OBJFUN). Instead of directly minimizing the OBJFUN, which can involve complex simulations or interactions with external software, NNO utilizes a faster optimization method, often a Genetic Algorithm (GA), to find the minimum of the trained ANN. The rationale behind this approach is that by optimizing the computationally efficient ANN, the algorithm can explore the solution space more extensively within a given computational budget, thereby increasing the likelihood of finding a good solution for the original OBJFUN. A key characteristic of NNO is its iterative nature. The ANN is not a static approximation; it is progressively refined through a series of steps involving evaluations of the real objective function at promising points identified by the optimization of the ANN. This iterative refinement allows the surrogate model to become more accurate over time, guiding the optimization process towards the true minimum of the OBJFUN. The effectiveness of NNO is predicated on the ANN's ability to learn and generalize the complex relationships inherent in the OBJFUN. Genetic Algorithms are particularly well-suited for optimizing ANNs due to their capacity to handle non-differentiable functions and navigate large, complex search spaces, which are typical features of the parameter space of neural networks.

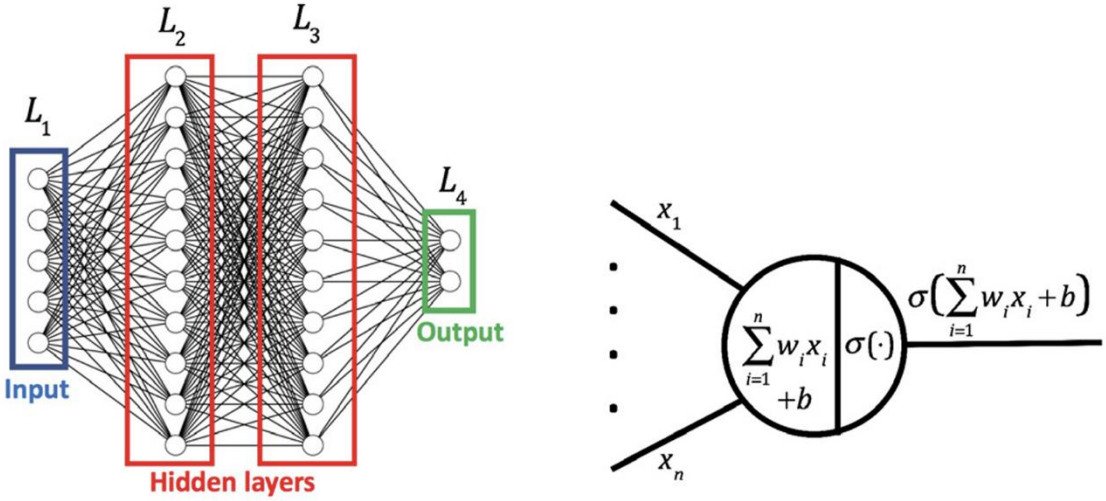

Figure 3.1 (a) Schematic of Neural Network (NN) (b) Schematic of a single neuron

3.3 Step-by-Step Explanation of the NNO Process

The Neural Network Optimization (NNO) algorithm follows a well-defined iterative process to find the minimum of a computationally expensive objective function. The optimization procedure goes as follows:

I. An initial set of training data is produced based on OBJFUN
II. The ANN is trained based on the above data set.
III. The ANN is used as an objective function in GA and is minimized.
IV. OBJFUN is evaluated at the optimum solution that is found by GA.
V. This extra data is added at the initial set of training data, thus extending the data by one additional OBJFUN function evaluation.
VI. Replace the initial training data with the extended training data
VII. Continue with step II above

3.3.1 Initial Data Collection

The process starts with the evaluation of the actual objective function (OBJFUN) at a small, carefully selected set of initial input values. This initial sampling is crucial as it generates the first training dataset that the Artificial Neural Network (ANN) will learn from. The selection of these initial data points is important to provide the ANN with a foundational understanding of the OBJFUN's behavior across the relevant input space. The quality and distribution of this initial data significantly influence the ANN's initial accuracy and the efficiency of the subsequent optimization process. If these initial samples fail to represent the key characteristics of the OBJFUN, the ANN might learn an inaccurate approximation, potentially leading the optimization towards less promising areas.

3.3.2 ANN Training

Once the initial dataset is collected, it is used to train the Artificial Neural Network (ANN). The primary goal of this training phase is for the ANN to learn the underlying mapping between the input values and the corresponding output values produced by the objective function (OBJFUN). This essentially creates a computationally cheaper approximation of the OBJFUN's behavior. The training process involves adjusting the internal parameters of the ANN, namely its weights and biases, to minimize the prediction error on the training data. Key

aspects of ANN training include selecting an appropriate ANN architecture (e.g., feedforward, convolutional, recurrent) based on the nature of the OBJFUN , choosing suitable activation functions for the neurons, defining a loss function to quantify the discrepancy between the ANN's predictions and the actual OBJFUN outputs, and selecting an optimization algorithm (e.g., gradient descent, Adam, RMSprop) to update the ANN's parameters during training. It is also crucial to employ validation techniques, such as splitting the data into training and validation sets, to monitor the ANN's performance on unseen data and prevent overfitting, which occurs when the ANN learns the training data too well but fails to generalize to new inputs. The choice of ANN architecture should align with the complexity and characteristics of the objective function being approximated.

3.3.3 Optimization with ANN

Instead of directly minimizing the computationally expensive OBJFUN, the algorithm proceeds to use a faster optimization method, typically a Genetic Algorithm (GA), to find the minimum of the trained ANN. Genetic Algorithms are population-based metaheuristic optimization techniques inspired by natural selection. They work by initializing a population of candidate solutions, evaluating their fitness using a fitness function (in NNO, this is the output of the ANN for a given input), selecting the fittest individuals to become parents, applying crossover to create new offspring, and introducing mutations to maintain diversity. In the context of NNO, the GA explores different input values and uses the ANN to quickly estimate the corresponding output, efficiently searching for input values that lead to the minimum output according to the ANN surrogate. The use of GA is advantageous here because it can handle non-differentiable and discontinuous functions, which the ANN might represent, and it is effective in exploring large and complex search spaces, reducing the risk of getting trapped in local minima. The choice of GA parameters, such as population size, mutation rate, and crossover rate, can significantly influence the GA's performance in finding the minimum of the ANN. By utilizing the ANN as a proxy, the GA can perform many more evaluations of potential solutions compared to directly evaluating the OBJFUN, leading to a more thorough exploration of the search space within a given computational budget.

3.3.4 Validation with Real Function

Once the Genetic Algorithm (GA) identifies a potential optimal solution (a set of input values) based on the Artificial Neural Network's (ANN) predictions, this solution is then used to evaluate the actual objective function (OBJFUN). This validation step is crucial to verify how well the ANN's prediction matches the true output value of the OBJFUN at the identified input. It helps to ensure that the optimization process remains aligned with the true objective and that the ANN's approximation is reasonably accurate in the vicinity of the promising solution found by optimizing the surrogate. The discrepancy between the ANN's prediction and the actual OBJFUN value at the validated point provides important information about the accuracy of the surrogate model in the region of interest.

3.3.5 Data Augmentation

The newly evaluated data point, consisting of the input found by the GA and its corresponding output from the OBJFUN, is then added to the existing training dataset. This data augmentation process expands the information that the ANN has learned about the OBJFUN's behavior, particularly in regions of the input space that the optimization process has deemed promising. By including a real evaluation of the OBJFUN at a point identified as potentially optimal by

the GA using the ANN surrogate, the augmented dataset can help improve the ANN's representation of the objective function in critical areas of the search space where the true minimum might lie. This targeted addition of data points is a form of active learning, focusing computational effort on improving the surrogate model's accuracy in relevant regions.

3.3.6 Iterative Refinement

Following data augmentation, the algorithm repeats the process from step 2. The ANN is retrained using the expanded dataset, which now includes the newly acquired information about OBJFUN's behavior. This retrained ANN has the potential to be a more accurate representation of the OBJFUN, especially in the regions of the search space being actively explored. The Genetic Algorithm (GA) then minimizes this updated ANN, and the best solution found is again validated by evaluating the real OBJFUN. This iterative cycle of retraining the ANN with augmented data and optimizing it with the GA continues, gradually refining the ANN's approximation of the OBJFUN and guiding the optimization process towards the true minimum of the objective function. The feedback loop between optimizing the ANN and evaluating the OBJFUN allows the algorithm to adapt and improve its search over time, focusing computational effort on the most promising areas of the search space.

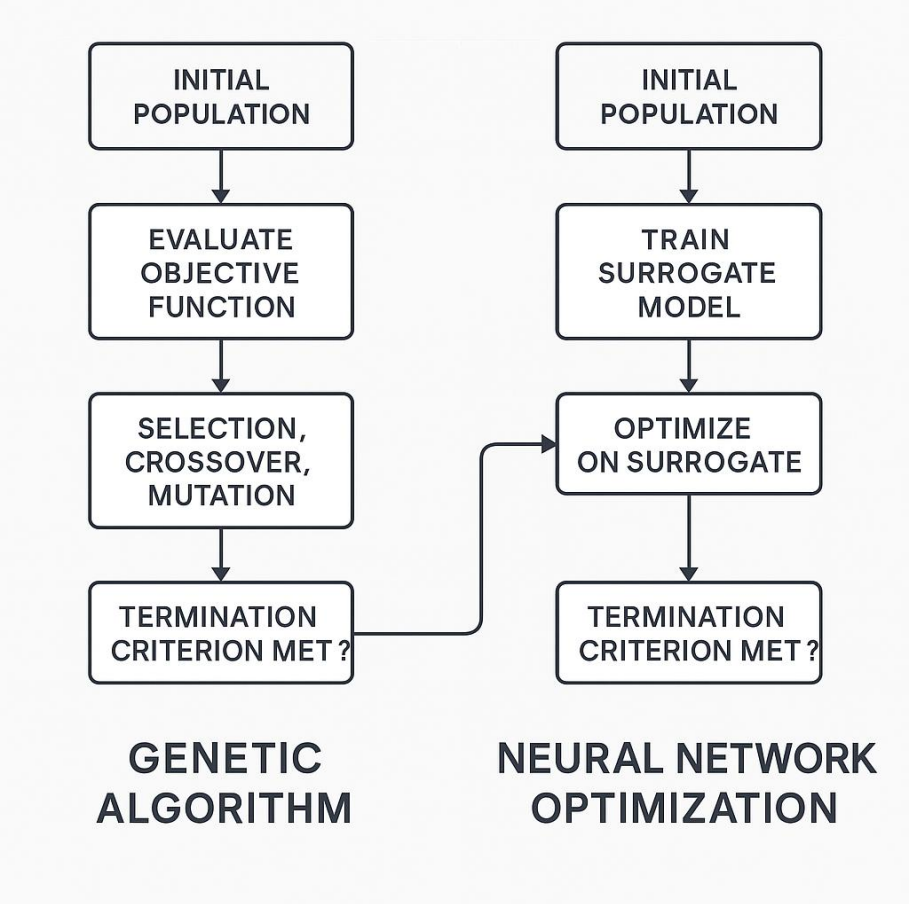

Figure 3.2 Methodology implemented

3.4 The Role of Artificial Neural Networks in NNO

Artificial Neural Networks (ANNs) are particularly well-suited for serving as surrogate models in optimization due to their inherent capabilities in learning and approximating complex, nonlinear relationships between inputs and outputs. This is achieved without requiring explicit knowledge of the underlying mathematical form of the objective function, making them invaluable when dealing with "black-box" functions derived from complex simulations or third-party software. The universal approximation theorem provides a theoretical basis for this, suggesting that ANNs with sufficient complexity can approximate any continuous function to a desired degree of accuracy. In the context of Neural Network Optimization (NNO), various types of ANN architecture can be employed depending on the characteristics of the objective function and the problem domain. Feedforward neural networks, also known as Multi-Layer Perceptrons (MLPs), are a common choice for general regression tasks. For problems where the input has a grid-like structure, such as spatial parameters, Convolutional Neural Networks (CNNs) can be effective due to their ability to learn hierarchical features. In cases involving sequential input data or objective functions with memory, Recurrent Neural Networks (RNNs) might be more appropriate. The selection of the most suitable ANN architecture is a critical step in NNO, as the complexity and structure of the ANN should be sufficient to capture the OBJFUN's behavior accurately without leading to overfitting, especially given the typically limited amount of initial training data. The flexibility offered by the diverse range of ANN architectures allows NNO to be adapted to a wide variety of optimization problems with varying degrees of complexity and data structures. However, the training process is equally critical, and the quality of the resulting surrogate model directly impacts the performance of the overall NNO algorithm. Factors such as the size and representativeness of the training data, the choice of architecture and training algorithm, and hyperparameter tuning all play a significant role in determining the accuracy and reliability of the ANN surrogate.

3.5 The Role of Genetic Algorithms in NNO

Genetic Algorithms (GAs) are a class of population-based metaheuristic optimization techniques inspired by the process of natural selection and genetic evolution. In the context of Neural Network Optimization (NNO), GA plays a crucial role in efficiently searching for the minimum of the Artificial Neural Network (ANN) surrogate. A GA operates on a population of candidate solutions, often represented as vectors of parameters called chromosomes. Each chromosome is evaluated based on its fitness, which in NNO is typically the output of the trained ANN for the corresponding input vector. The algorithm then proceeds through an iterative process of selection, crossover, and mutation to evolve the population towards better solutions. Selection involves choosing individuals with higher fitness (lower ANN output in minimization) to become parents for the next generation, using methods like roulette wheel selection or tournament selection. Crossover, or recombination, combines the genetic information of two selected parents to create new offspring by exchanging parts of their chromosomes, using techniques such as one-point or two-point crossover. Mutation introduces small random changes to the genes (parameters) of the offspring to maintain diversity in the population and explore new regions of the search space, often using operators like bit-flip or Gaussian mutation. The use of GAs for optimizing the ANN surrogate in NNO offers several advantages. Notably, GAs can effectively handle non-differentiable and discontinuous objective functions, which the ANN might represent. They are also adept at exploring large and complex search spaces, reducing the risk of getting trapped in local minima, a common issue

with gradient-based methods. Furthermore, the inherent parallelism of GAs, where the fitness of everyone in the population can be evaluated independently, allows for potential speedups in computation. The stochastic nature of GAs contributes to a more robust search, especially in the presence of multiple local optima in the ANN's representation of the OBJFUN. However, the effectiveness of the GA in NNO is highly dependent on the appropriate selection of its parameters, such as population size, crossover rate, and mutation rate, which control the crucial balance between exploration and exploitation of the search space.

3.6 Advantages of the NNO Technique

The Neural Network Optimization (NNO) technique offers several compelling advantages for tackling complex optimization problems, particularly those involving computationally expensive objective functions:

- Reduced Computational Cost: The most significant benefit of NNO is the substantial reduction in the number of evaluations required for the computationally expensive real objective function (OBJFUN). The Genetic Algorithm (GA), which drives the optimization process, primarily interacts with the much faster Artificial Neural Network (ANN) surrogate. This allows for a far greater number of candidate solutions to be explored within a given computational budget compared to directly optimizing the OBJFUN.
- Efficient Exploration of Solution Space: The utilization of a Genetic Algorithm (GA) enables a broad and efficient exploration of the potentially vast and complex solution space. GA is known for their ability to avoid getting trapped in local optima, increasing the likelihood of finding a global or near-global optimum, especially in problems where the objective function landscape is rugged and contains multiple local minima.
- Applicability to Complex Problems: NNO is particularly well-suited for optimization problems where the objective function exhibits characteristics that make traditional methods struggle. This includes cases where the OBJFUN is nonlinear, non-differentiable, discontinuous, or involves complex simulations or interactions with third-party software, making direct gradient-based optimization challenging or even infeasible.
- Iterative Refinement: The iterative nature of NNO, where the ANN surrogate is continuously trained and refined based on evaluations of the real objective function at promising points identified by the GA, leads to improved accuracy of the surrogate model in the regions of interest. This iterative process can result in better convergence towards the true optimum over time as the ANN becomes a more faithful representation of the OBJFUN.

The ability of NNO to significantly reduce the computational burden associated with expensive objective function evaluations makes it a practical approach for problems that would otherwise be intractable. The synergistic combination of ANNs for efficient function approximation and GAs for robust global search leverages the strengths of both techniques, providing a powerful framework for tackling complex optimization challenges.

3.7 Limitations and Considerations

While the Neural Network Optimization (NNO) technique offers significant advantages, it also has certain limitations and considerations that need to be considered when applying it to optimization problems:

- Accuracy of the ANN Surrogate: The success of NNO is highly dependent on the Artificial Neural Network's (ANN) ability to accurately approximate the objective function (OBJFUN). If the ANN surrogate is not a faithful representation of the OBJFUN, the optimum found by optimizing the ANN might not correspond to the true optimum of the OBJFUN.
- Choice of ANN Architecture and Training: Selecting an appropriate ANN architecture and training effectively can be a challenging process that often requires domain expertise and experimentation. Factors such as the number of layers and neurons, the choice of activation functions, and the training algorithm and its hyperparameters need to be carefully considered to ensure the ANN learns the underlying relationships in the data without overfitting or underfitting.
- Choice of GA Parameters: The performance of the Genetic Algorithm (GA) within NNO is sensitive to the selection of its parameters, including population size, mutation rate, crossover rate, and selection method. Poorly chosen parameters can lead to slow convergence, premature convergence to local optima of the ANN, or inefficient exploration of the search space.
- Computational Cost of Initial Sampling and ANN Training: Although NNO aims to reduce the overall computational cost, the initial data collection phase, which involves evaluating the real OBJFUN at a set of initial points, and the subsequent training of the ANN can still be computationally intensive, especially for high-dimensional problems or when a large amount of initial data is required to train an accurate surrogate.
- Convergence Criteria: Determining when the NNO algorithm has converged to a satisfactory solution can be less straightforward compared to some traditional optimization methods. Surrogate optimization techniques might require different stopping criteria, such as a maximum number of iterations or function evaluations, or monitoring the improvement in the best solution over time.
- Potential for Local Optima: While Genetic Algorithms are generally better at avoiding local optima than gradient-based methods, there is still a possibility that the NNO process might converge to a local minimum of the objective function if the ANN surrogate is not sufficiently accurate in representing the global landscape of the OBJFUN or if the GA's search is not exhaustive enough.

There exists a trade-off between the complexity and accuracy of the ANN surrogate and the computational resources required to train it. Furthermore, the performance of NNO can be influenced by the specific characteristics of the objective function, such as its dimensionality, degree of nonlinearity, and the presence of noise.

4 Theoretical Background

To gain a clear understanding of the system's behavior, we begin by modeling a single-degree-of-freedom (SDOF) system incorporating the Bouc-Wen hysteresis model to account for nonlinearities. This preliminary step allows us to explore the fundamental dynamics introduced by nonlinear behavior and to study how the Bouc-Wen parameters influence the system's response. Through this analysis, we aim to calibrate the model parameters to match experimental data as closely as possible, thereby validating the effectiveness of the chosen nonlinear formulation.

Once the SDOF model is established and understood, we proceed to test the Neural Network Optimization (NNO). We implement NNO on the simplified system to evaluate its performance in parameter identification and optimization. This phase is crucial to understand how the NNO behaves with nonlinear dynamic systems and to determine the appropriate configuration of the optimization's hyperparameters for robust and accurate convergence.

After successfully validating both the nonlinear model and the optimization technique on the SDOF system, we advanced to a more realistic two-degree-of-freedom (2DOF) model. This enhanced model better represents the actual dynamics of a Stockbridge damper, especially in capturing the coupled motion of the messenger cable and the damper mass. In addition to the Bouc-Wen nonlinearity, we also introduce a cubic stiffness term to more accurately replicate the nonlinear restoring forces observed in practice. This final step allows us to simulate the real-world behavior of the damper with higher reliability.

4.1 Single Degree of Freedom System

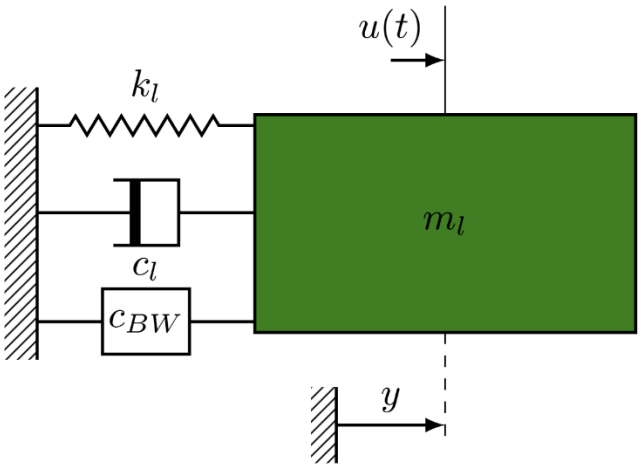

Figure 4.1 Schematic of SDOF system

The vibrations of a single-degree-of-freedom Bouc-Wen system, i.e. a Bouc-Wen oscillator with a single mass, is shown in Figure 4.1, and governed by Newtons law of dynamics written in the form

$$m_l\,\ddot{y}(t) + r(y,\dot{y}) + z(y,\dot{y}) = u(t)$$

where m_l is the mass constant, y the displacement, u the external force, and where an over-dot indicates a derivative with respect to the time variable t. The total restoring force in the system is composed of a static nonlinear term $r(y,\dot{y})$, which only depends on the instantaneous values

of the displacement $y(t)$ and velocity $\dot{y}(t)$, and of a dynamic, i.e. history-dependent, nonlinear term $z(y, \dot{y})$, which encodes the hysteretic memory of the system. In the present study, the static restoring force contribution is assumed to be linear, that is

$$r(y, \dot{y}) = k_l\, y + c_l\, \dot{y}$$

where k_l and c_l are the linear stiffness and viscous damping coefficient, respectively. This linear term acts as a baseline model to contrast the additional nonlinear effects introduced by $z(y, \dot{y})$. In practical systems, this might represent the basic mechanical response without considering internal friction or hysteresis. The hysteretic force $z(y, \dot{y})$ obeys the first-order differential equation

$$\dot{z}(y, \dot{y}) = \alpha\, \dot{y} + \beta(\gamma\, |\dot{y}|\, |z|^{\nu-1}\, z + \delta\, \dot{y}\, |z|^{\nu})$$

where the five Bouc-Wen parameters α, β, γ, δ and ν are used to tune the shape and the smoothness of the system hysteresis loop.

The Bouc-Wen model introduces a first-order differential equation for z, allowing it to represent complex hysteresis loops seen in mechanical systems. The parameters have distinct effects:

- α scales the direct input effect.
- β, γ, and δ together shape the nonlinearity and rate of energy dissipation.
- ν controls the smoothness of the hysteresis transition. Low values result in rounded loops; high values approach ideal elasto-plastic behavior.

Physical parameters and the experimental data are being implemented from [28]. Table 4.1 lists the values of the physical parameters selected in this study. The linear modal parameters deduced from m_l, k_l and c_l are given in Table 4.2. Figure 4.2 (a) illustrates the existence of a non-degenerate loop in the system input-output plane for quasi-static forcing conditions. In comparison, by setting the parameter β to 0, linear behavior is retrieved in Figure 4.2 (b).

Parameters	m_l	c_l	k_l	α	β	γ	δ	ν
Value	2	10	5e4	5e4	1e3	0.8	-1.1	1

Table 4.1 Physical parameters

Parameters	Natural frequency $\omega_0\ (Hz)$	Damping ratio ζ (%)
Value	35.59	1.12

Table 4.2 Modal parameters

Physically, the hysteretic term $z(y, \dot{y})$ captures energy dissipation mechanisms not explainable by pure viscous damping—such as inter-strand friction in cables or micro-slipping. This makes it highly suitable for modeling devices like Stockbridge dampers where such effects are dominant.

The Bouc-Wen model is chosen for its balance between mathematical tractability and flexibility in capturing diverse hysteretic behaviors. It allows for easy tuning to replicate experimental

loops and is integrable with numerical solvers like the Newmark method, making it well-suited for both simulation and optimization.

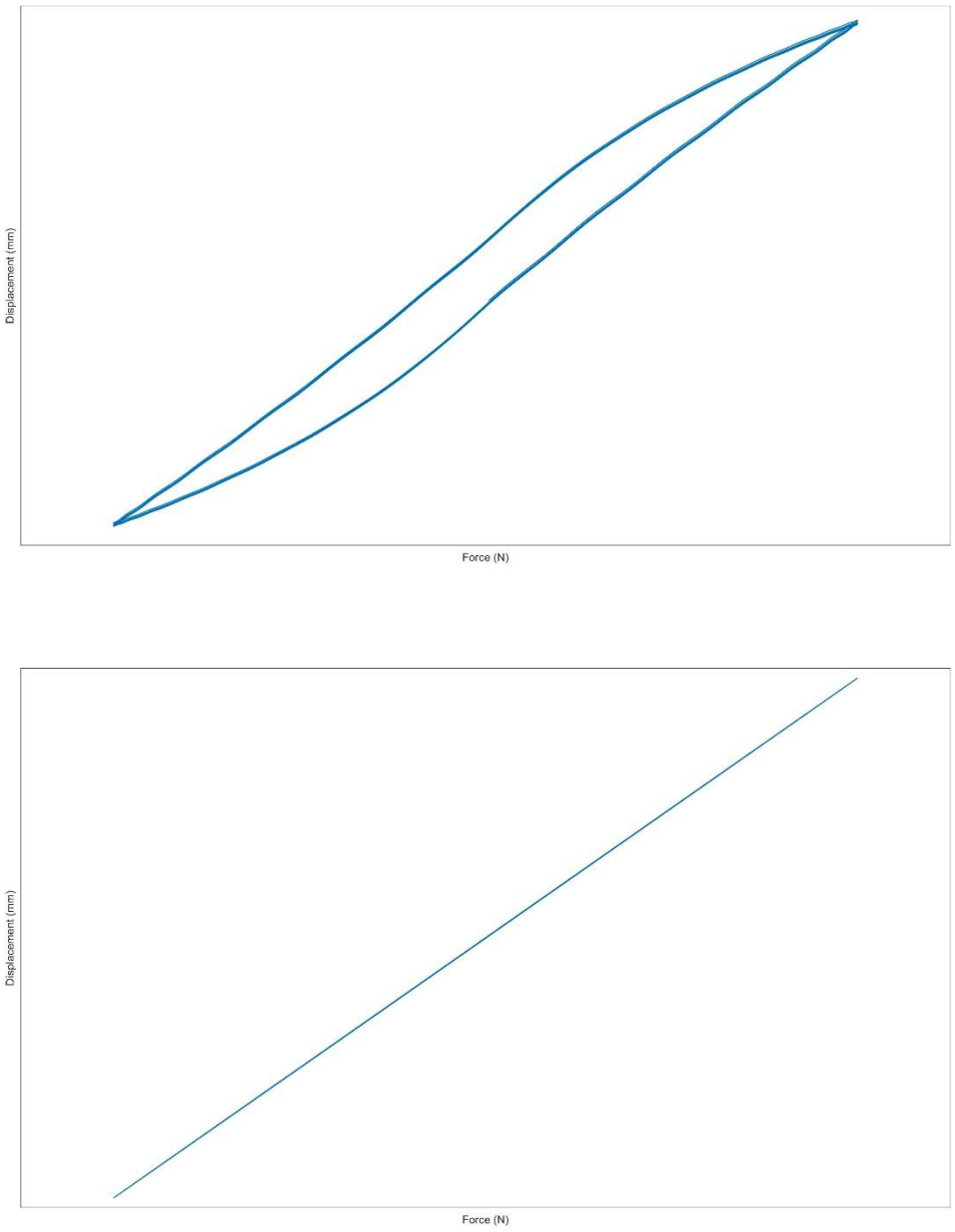

Figure 4.2 Hysteresis loop in the system input-output plane (a) non-degenerate loop obtained for the parameters in Table 1; (b) linear behavior retrieved when setting the parameter to 0.

The excitation $u(t)$ in these two figures is a sine wave with a frequency of 1 Hz and an amplitude of 120 N. The response exhibits no initial condition transients as it depicted over 10 cycles in the steady state. The input excitation and the output signal regarding the Bouc-Wen model is as it is seen in the Figure 4.3.

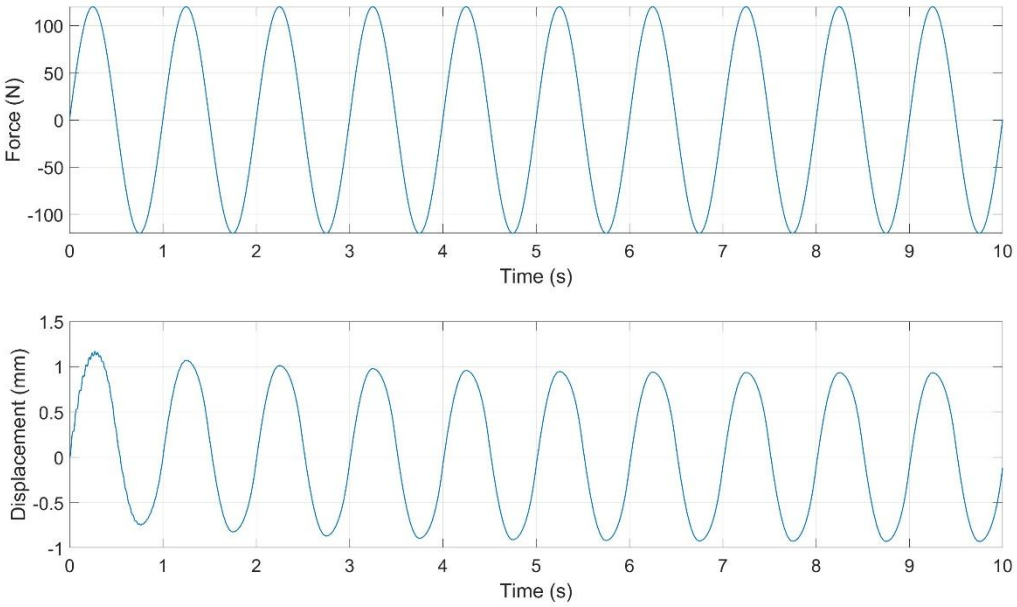

Figure 4.3 Top: Sine input excitation. Bottom: Output displacement

The Bouc-Wen dynamics in Equations. (1) and (3) can be effectively integrated in time using a Newmark method. Newmark integration relies on one-step-ahead approximations of the velocity and displacement fields obtained by applying Taylor expansion and numerical quadrature techniques. Denoting by h the integration time step, these approximation relations write

$$\dot{y}(t+h) = \dot{y}(t) + (1-a)\, h\, \ddot{y}(t) + a\, h\, \ddot{y}(t+h)$$

$$y(t+h) = y(t) + h\, \dot{y}(t) + (0.5-b)h^2\, \ddot{y}(t) + b\, h^2 \ddot{y}(t+h)$$

Parameters a and b are typically set to 0.5 and 0.25, respectively. Equations. (4) are herein enriched with an integration formula for the variable $z(t)$, which takes the form

$$z(t+h) = z(t) + (1-c)\, h\, \dot{z}(t) + c\, h\, \dot{z}(t+h)$$

where c, similarly to a, is set to 0.5. Based on Equations. (4) and (5), a Newmark scheme proceeds in two steps. First, predictions of $\dot{y}(t+h)$, $y(t+h)$ and $z(t+h)$ are calculated assuming $\ddot{y}(t+h) = 0$ and $z(t+h) = 0$. Second, the initial predictors are corrected via Newton-Raphson iterations to satisfy the dynamic equilibria in Equations. (1) and (3).

4.1.1 Results of the System in Case of Sine Sweep Excitation

The excitation $u(t)$ in this case is a sine sweep with the same amplitude as the sine excitation (A=120 N). The starting and ending frequency are respectively 0 Hz and 60 Hz and the sweep rate is chosen 0.5 Hz/s.

The physical parameters of the system stay the same as the previous model.

Figure 4.4 and Figure 4.5 respectively show excitation and the result displacement over time and instant frequency.

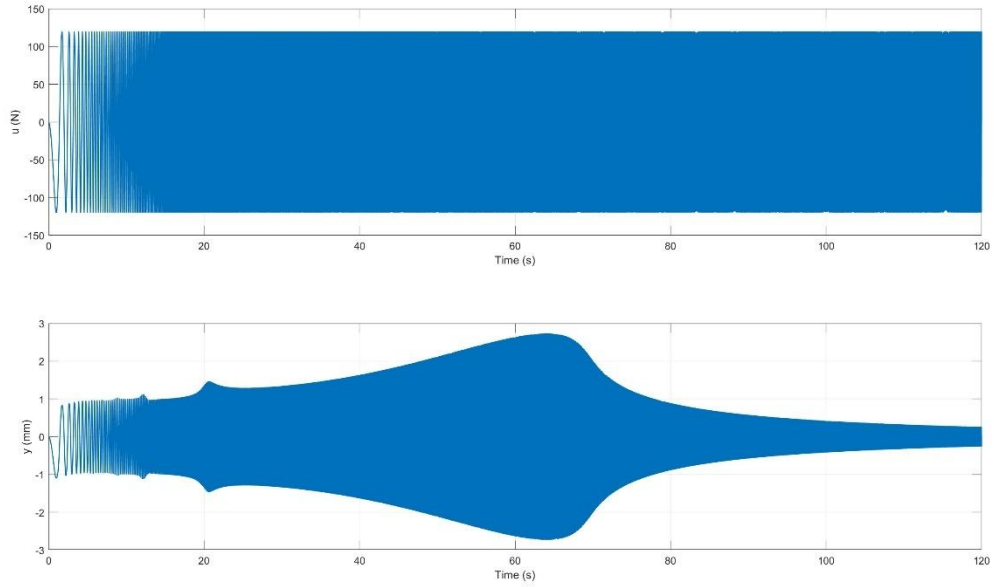

Figure 4.4 Sine sweep input and output displacement in time domain

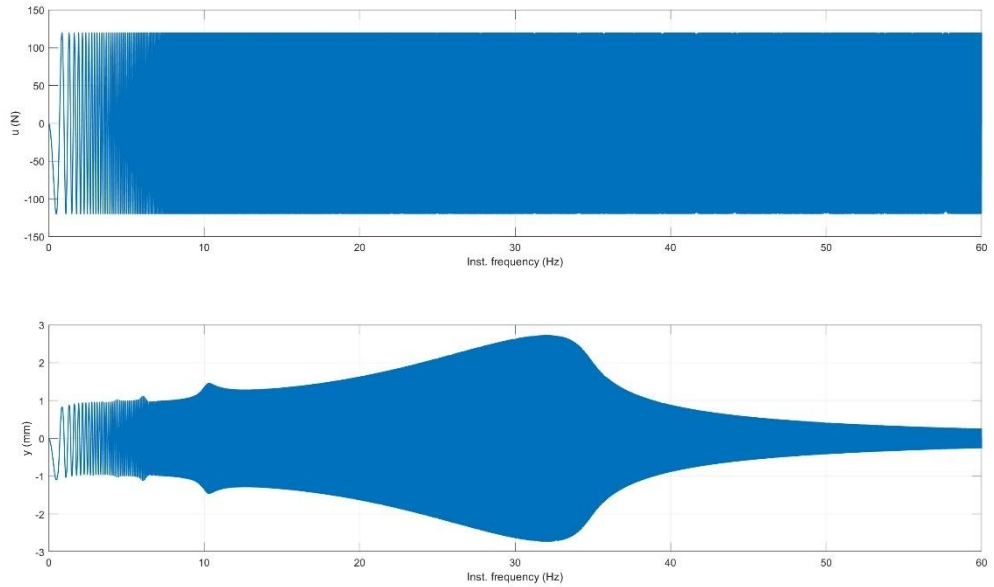

Figure 4.5 Sine sweep input and output displacement in instant frequency domain

Figure 4.6 is a spectrogram of the signal y, representing how the signal's frequency content evolves over time. The x-axis shows time in minutes, the y-axis shows frequency in Hertz (Hz), and the color scale represents power intensity in decibels per Hertz (dB/Hz), with yellow indicating higher power and dark blue representing lower power.

There are several clear, increasing-frequency bands over time, suggesting frequency components that grow linearly because of the chirp signal.

Harmonics are visible above this main band, reinforcing the presence of structured, periodic components in the signal.

Overall, this spectrogram reveals non-stationary behavior with time-varying frequencies and consistent harmonic structures.

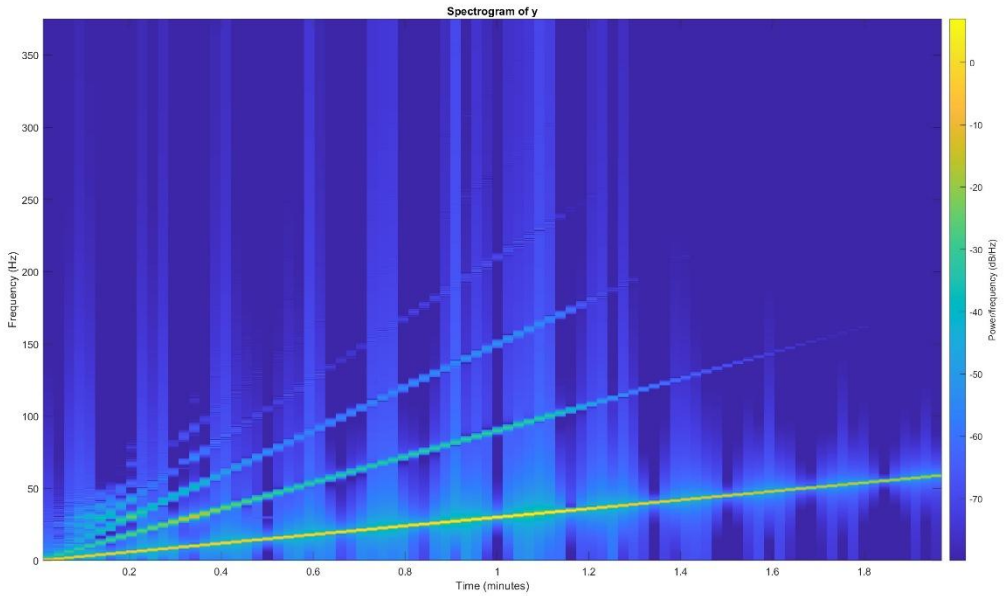

Figure 4.6 Spectrum of signal y

Hysteresis loop in the system input-output plane is shown in Figure 4.7 in the different frequency ranges.

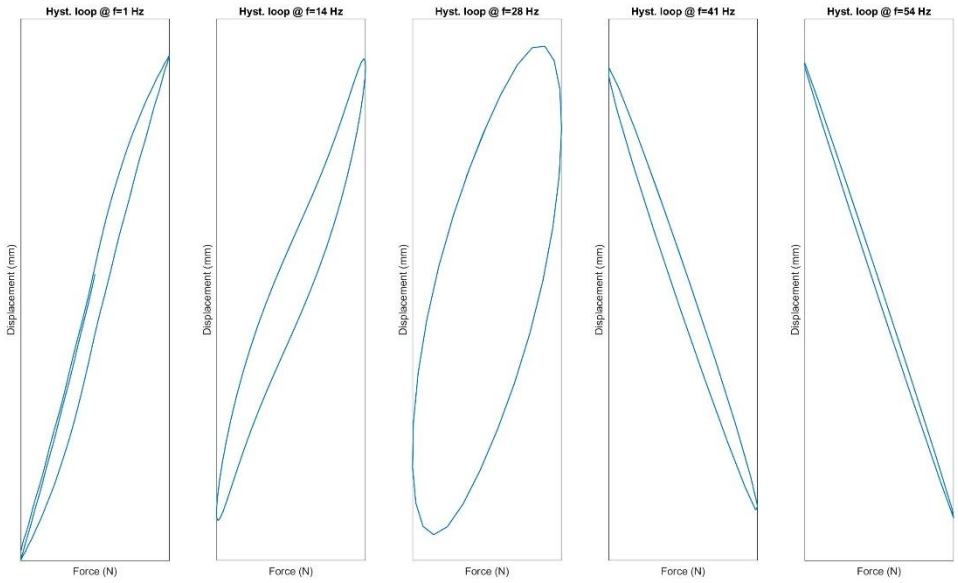

Figure 4.7 Hysteresis loop in the system input-output plane in different frequencies. Left to right: 1 Hz, 14 Hz, 28 Hz, 41 Hz, and 54 Hz

Figure 4.8 is the representation of the resultant PSD of the system.

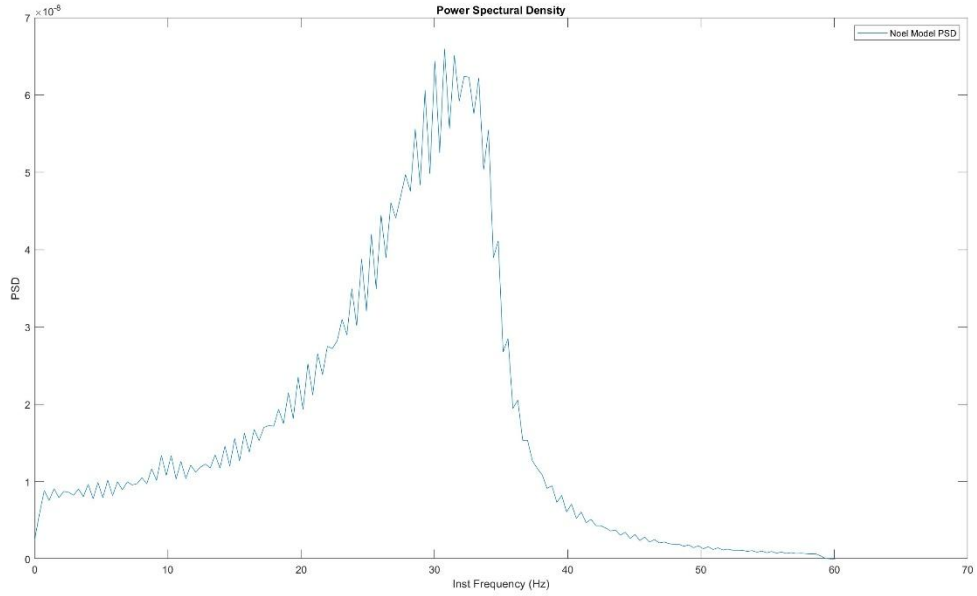

Figure 4.8 PSD of displacement

4.2 Two Degree of Freedom System

After validating the nonlinear dynamic response using a single-degree-of-freedom model, a more realistic two-degree-of-freedom (2DOF) system is introduced to approximate the dynamics of a real Stockbridge damper more closely. This model allows investigation of coupled mass interactions, distributed damping, and nonlinear stiffness, mimicking the interaction between the messenger cable and the weights.

Two-degree-of-freedom system is analyzed in four different configurations:

- Bouc-Wen damper at the second DOF
- Bouc-Wen damper between the first and second DOF
- Bouc-Wen damper and the cubic stiffness damper at the second DOF
- Bouc-Wen damper and the cubic stiffness damper between the first and second DOF

The four configurations aim to systematically examine how the location and type of nonlinearity (Bouc-Wen hysteresis and cubic stiffness) affect the system's vibrational response. Each setup highlights different energy dissipation and stiffness behaviors, which are key to optimizing damper design.

The system consists of:

- Two masses: m_1 and m_2
- Linear stiffness elements: k_1, k_2, k_{12}
- Proportional viscous damping elements: c_1, c_2, c_{12}
- A Bouc-Wen hysteretic damper
- A cubic stiffness spring
- An external force f(t) applied to m_1

The governing equations of motion for the system are given by:

$$M\ddot{y} + C_v\dot{y} + Ky + F_{nl} = F$$

where:

- M is the mass matrix.
- C_v is the proportional viscous damping matrix.
- K is the linear stiffness matrix.
- F_{nl} is the vector of nonlinear forces.
- F is the external force vector.

The displacement, velocity, and acceleration vectors are defined as:

$$y = \begin{bmatrix} y_1 \\ y_2 \end{bmatrix}, \qquad \dot{y} = \begin{bmatrix} \dot{y}_1 \\ \dot{y}_2 \end{bmatrix}, \qquad \ddot{y} = \begin{bmatrix} \ddot{y}_1 \\ \ddot{y}_2 \end{bmatrix}$$

The external force is:

$$F = \begin{bmatrix} F(t) \\ 0 \end{bmatrix}$$

The Bouc-Wen model introduces hysteretic effects in the force-displacement relationship of the damper. The force contribution from the Bouc-Wen damper, z, is given by:

$$F_{BW} = z$$

where z is the hysteretic variable governed by:

$$\dot{z} = \alpha\dot{y} - \beta(\gamma|\dot{y}||z|^{\nu-1}z + \delta\dot{y}|z|^{\nu})$$

The cubic stiffness nonlinearity contributes a restoring force of the form:

$$F_{cubic} = k_{nl}y_2^3$$

where k_{nl} is the coefficient of nonlinear stiffness.

The nonlinear force vector is expressed as:

$$F_{NL} = \sum_{j=1}^{2} \mu_j \, L_j \, g_j$$

where:

- μ_j are coefficients of nonlinear functions.
- L_j are Boolean vectors defining the location of the nonlinearities.
- g_j represent nonlinear basis functions.

For this system:

$$F_{NL} = \begin{bmatrix} 0 \\ F_{BW} + F_{cubic} \end{bmatrix}$$

Physical and Bouc-Wen parameters chosen to showcase the characteristics of the system are in Table 4.3 and Table 4.4. All these parameters carefully have been chosen and tuned only to check the nonlinearity characteristics and there is no experimental validation.

Parameters	m_1	m_2	k_1	k_2	k_{12}	c_1	c_2	c_{12}
values	0.5 kg	1 kg	2000 N/m	5000 N/m	500 N/m	5 N.s/m	2 N.s/m	1 N.s/m

Table 4.3 physical parameters of 2DoF system

Parameters	α	β	γ	δ	ν	k_{nl}
values	500	10	0.8	-1.1	2	1000

Table 4.4 Nonlinear parameters of 2DoF system

4.2.1 Bouc-Wen damper at the end

In this configuration, the Bouc-Wen nonlinear damper is attached between the second mass and ground. This mimics a scenario where the nonlinearity primarily affects the outer mass (similar to the weight of a Stockbridge damper), and the system dissipates energy only at one end as it is seen in Figure 4.9.

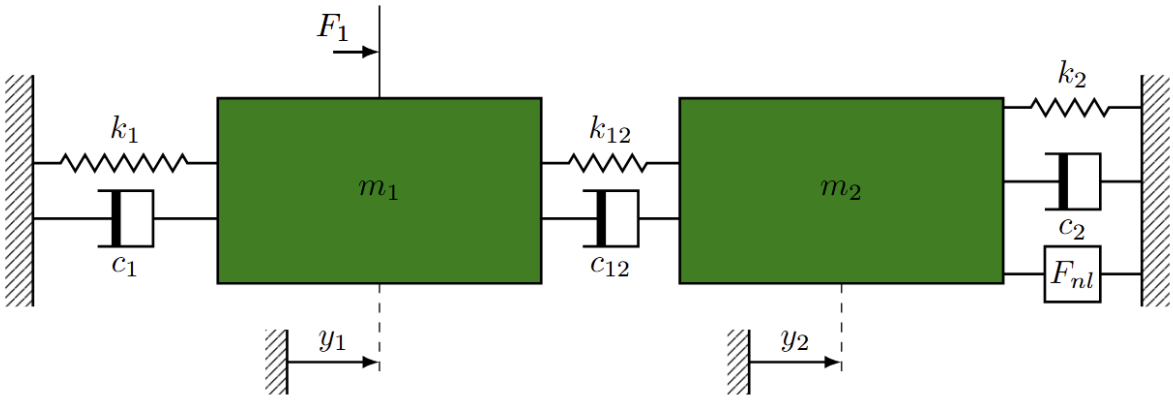

Figure 4.9 Schematic of 2dof system with nonlinear damping at the end

In this case nonlinear force would be:

$$F_{NL} = \begin{bmatrix} 0 \\ F_{BW} \end{bmatrix}$$

The results of the first configuration are in Figure 4.10:

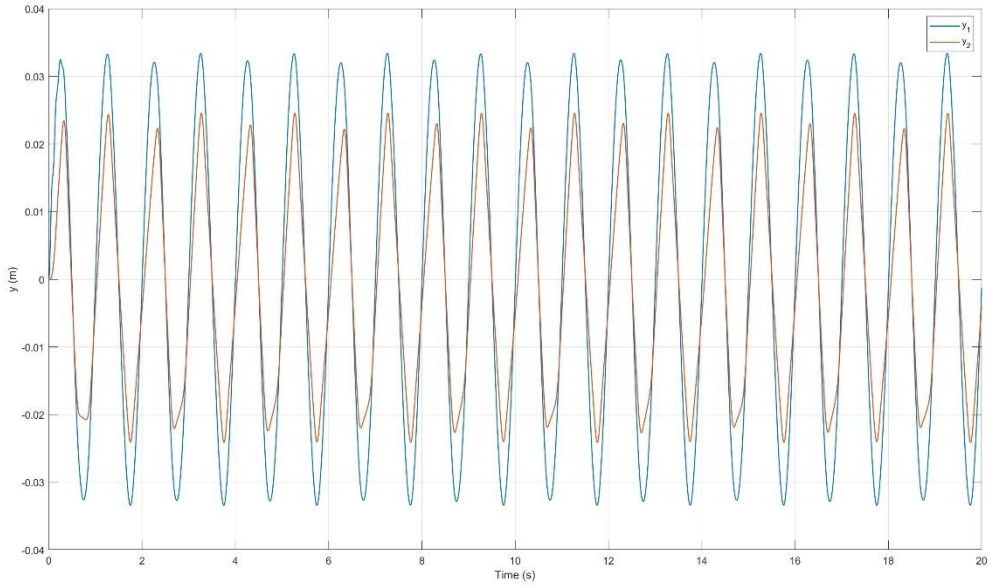

Figure 4.10 Displacements of first configuration of 2DoF system

The results in Figure 4.10 show how localized damping affects the second mass. The first mass exhibits larger oscillations due to its indirect coupling to the nonlinearity. This configuration helps isolate the contribution of boundary-localized hysteresis.

4.2.2 Bouc-Wen damper in the middle

In this case, the Bouc-Wen damper is placed between the two masses, modeling internal hysteresis that affects both degrees of freedom symmetrically as in Figure 4.11.

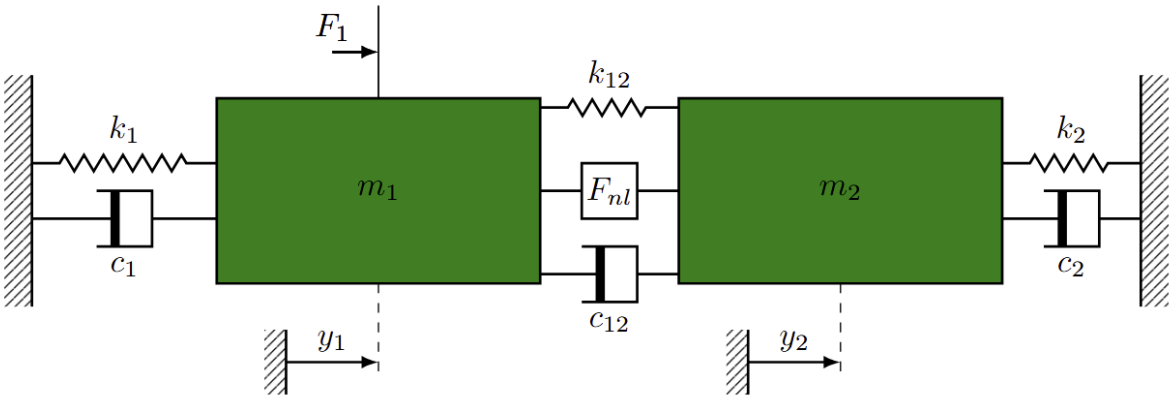

Figure 4.11 Schematic of 2dof system with nonlinear damping in the middle

The nonlinear force would change accordingly:

$$F_{NL} = \begin{bmatrix} F_{BW} \\ F_{BW} \end{bmatrix}$$

Figure 4.12 represents the output of the system in this case.

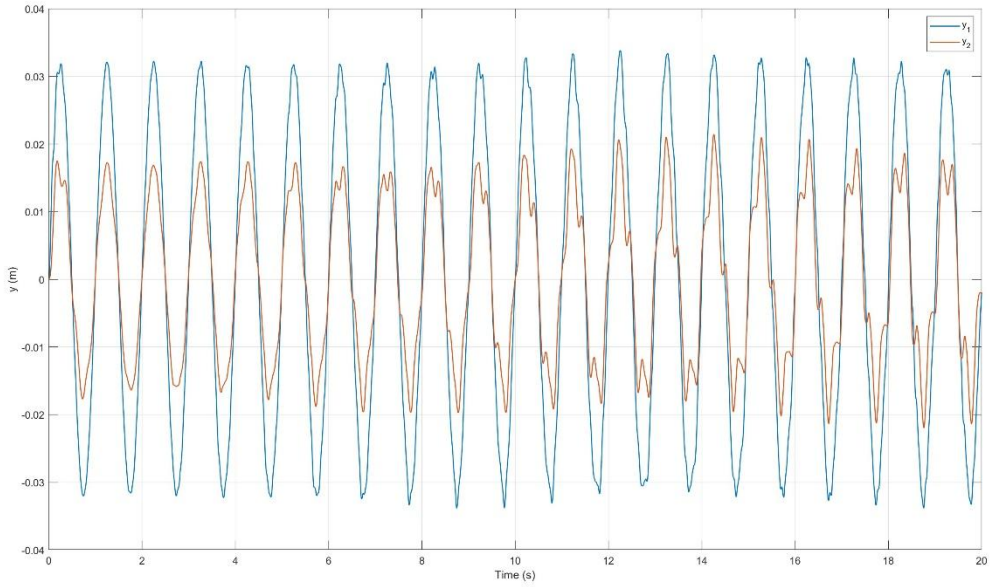

Figure 4.12 Displacements of the system in 2nd Configuration

As seen in Figure 3.12, both masses now experience direct damping forces. The system exhibits more balanced displacement profiles. This configuration simulates internal frictional behavior in the messenger cable between two vibrating weights and is expected to lead to more efficient energy dissipation.

4.2.3 Bouc-Wen damper and the cubic stiffness damper in the end

This configuration adds a nonlinear stiffness term (cubic spring) in parallel with the Bouc-Wen damper at the end. It mimics geometric stiffening effects, such as large deformations of the messenger cable, acting alongside hysteretic damping.

The schematic of the system is as in Figure 4.9 but the nonlinear force is different in this case and the cubic stiffness damper would be added to the nonlinear force:

$$F_{NL} = \begin{bmatrix} 0 \\ F_{BW} + F_{cubic} \end{bmatrix}$$

Figure 4.13 shows the results of the system in this configuration.

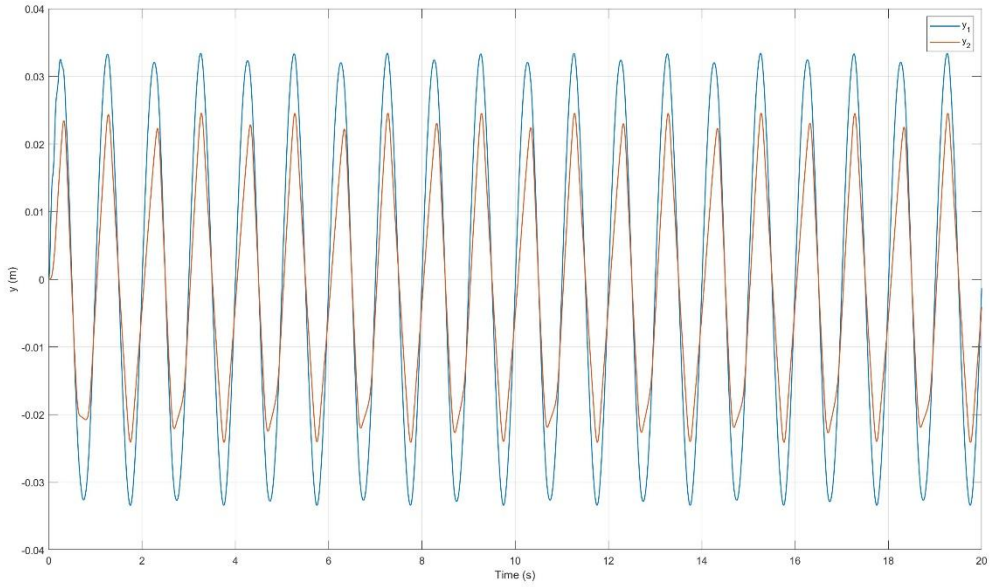

Figure 4.13 Displacements of the system in 3rd Configuration

Figure 3.13 shows the impact of geometric nonlinearity: increased resistance to large displacements and amplitude-dependent behavior. Combined with the hysteretic damper, the response is more complex, with possible hardening or softening effects depending on the excitation level.

4.2.4 Bouc-Wen damper and the cubic stiffness damper in the middle

The most complex case introduces both Bouc-Wen damping and cubic stiffness between the two masses, simulating nonlinear interactions internal to the damper structure—such as friction, material hysteresis, and geometric softening/hardening—all acting on both masses.

In the last case we have the system in Figure 4.11 with an addition of the cubic stiffness damper. So, the nonlinear force would be:

$$F_{NL} = \begin{bmatrix} F_{BW} + F_{cubic} \\ F_{BW} + F_{cubic} \end{bmatrix}$$

As the nonlinear force is in the middle, it is acting on both masses, and the resulting displacements would be as in Figure 4.14.

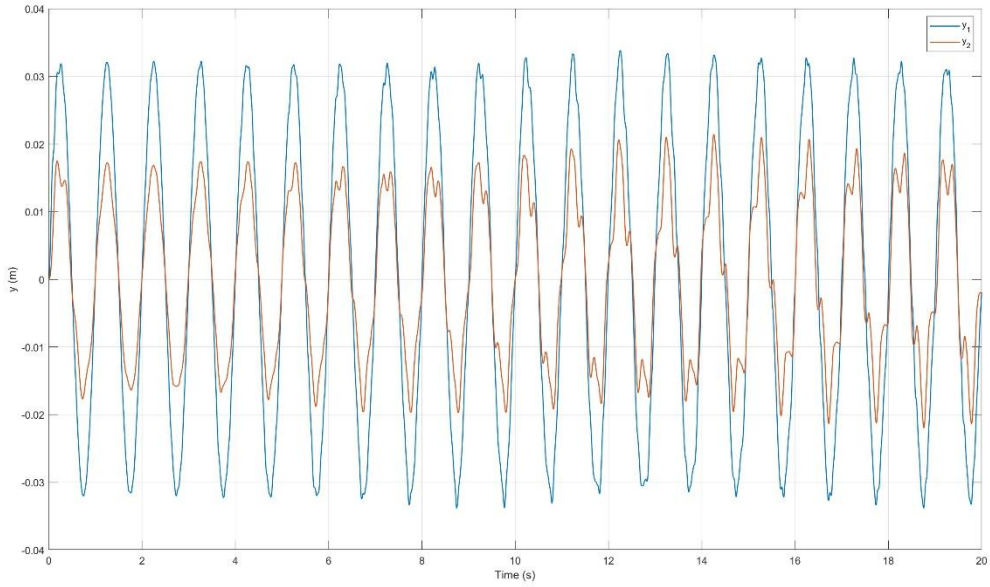

Figure 4.14 Displacements of the system in 4th Configuration

As shown in Figure 3.14, both masses are heavily influenced by the combined nonlinearities. This configuration demonstrates the full coupled dynamics of a nonlinear damper and is the most representative of real Stockbridge damper behavior.

4.3 Optimization of SDOF Bouc-Wen Parameters

The goal of this section is to assess the accuracy and efficiency of the proposed Neural Network Optimization (NNO) technique in estimating the Bouc-Wen model parameters for a single-degree-of-freedom (SDOF) nonlinear dynamic system. Using synthetic 'experimental' data from literature as a reference, the optimization process seeks to minimize the difference between the simulated system response and the reference response, measured in terms of the Power Spectral Density (PSD).

Physical parameters of the Bouc-Wen system in [28] are taken as our experimental model that our optimized data should be close to this data, and their relative difference (relative error) is the cost function for this optimization.

$$errorVec = \frac{PSD - Exp\_PSD}{Exp\_PSD}$$

NNO parameters are mentioned in the Table 4.5.

Parameters	Definition	Value
nVar	Number of design variables	4
initSim	Number of Abaqus analyses for initial training of the neural network	5
hiddenSizes	Number and size of hidden layers	15
Psize	Population size	10
funTol	Termination tolerance of error between target and simulated curve	0.0005
maxSim	Maximum number of iterations	60
XTol	Stall tolerance for X	0.001
YTol	Stall tolerance for Y	0.001

Table 4.5 NNO parameters

Design variables and their boundaries are in Table 4.6.

Variables	LB	UB
α	49900	50100
β	900	1100
γ	0.1	1
δ	-3	-0.1

Table 4.6 Design variables and their boundaries

The NNO process follows a surrogate-based optimization framework:

- Initial Data Generation: A small number of simulations are run using different Bouc-Wen parameters to train the initial ANN surrogate model.
- ANN Training: The ANN learns the mapping between Bouc-Wen parameters and PSD output.
- Optimization: The GA operates on the ANN surrogate to find promising parameter sets.
- Validation & Refinement: Promising candidates are evaluated with the full dynamic model, and the new data is used to retrain the ANN (active learning loop).
- Convergence Check: The process continues until convergence criteria are met (low error between simulated and target PSD).

The results of optimization and their comparison with the training data set variables are in Table 4.7.

Design parameters	J.P. Noel variables	Optimized values
α	50000	50026
β	1000	1020
γ	0.8	0.76
δ	-1.1	-1.14

Table 4.7 Experimental and optimized values

The results show that the optimized parameters are remarkably close to the reference values from [28], with relative errors of less than 5% across all variables. This close agreement demonstrates that the NNO technique can effectively recover the original system parameters, even with a limited number of high-fidelity simulations.

Figure 4.15 shows a comparison of the Power Spectral Density (PSD) between the two models. The dominant peak frequency and overall shape of the PSD curves align well, indicating that the energy distribution across frequency components is preserved by the optimized model. This suggests good dynamic fidelity.

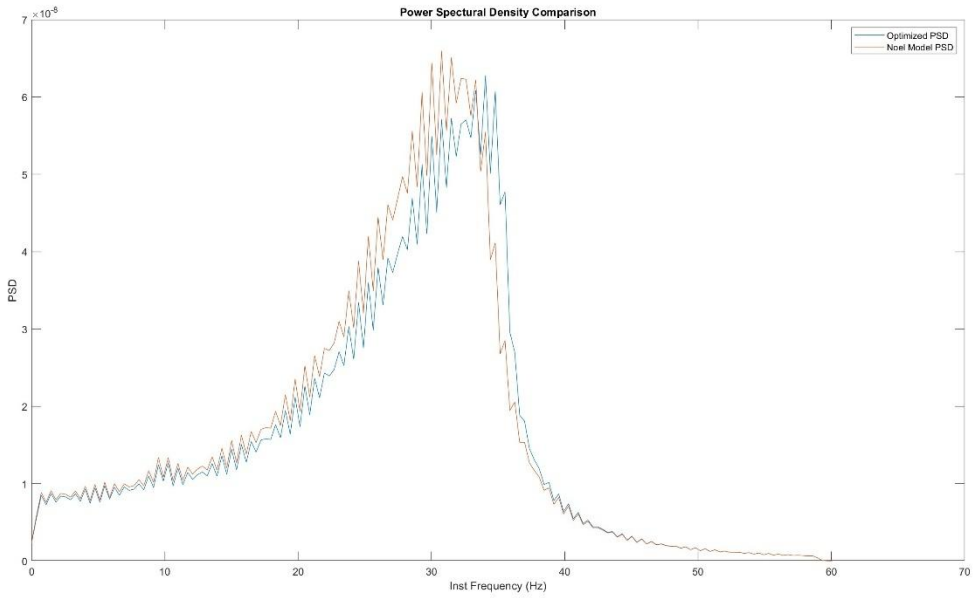

Figure 4.15 Comparison of the PSDs between experimental and optimized data

And the accuracy of the optimized model is shown in Figure 4.16 which is a representation of the displacement. The time-domain displacement signals show strong agreement in both amplitude and phase, further confirming the accuracy of the parameter identification.

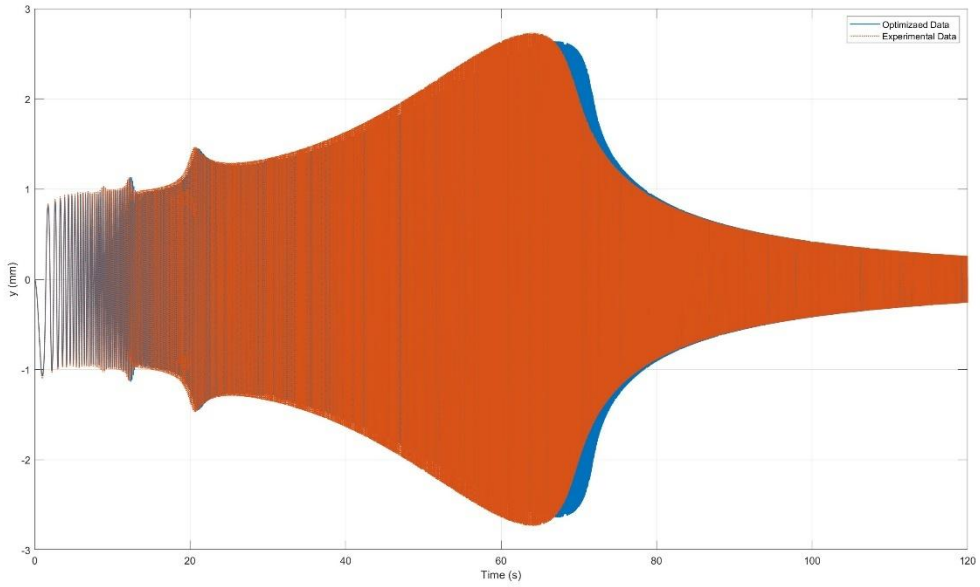

Figure 4.16 Displacement comparison of experimental and optimized data

The objective function error and the error of NNO during optimization are respectively in Figure 4.17 and Figure 4.18. The objective function error in Figure 4.17 decreases consistently, showing stable convergence. The ANN error in Figure 4.18 also decreases, indicating that the surrogate model becomes increasingly accurate as more samples are added.

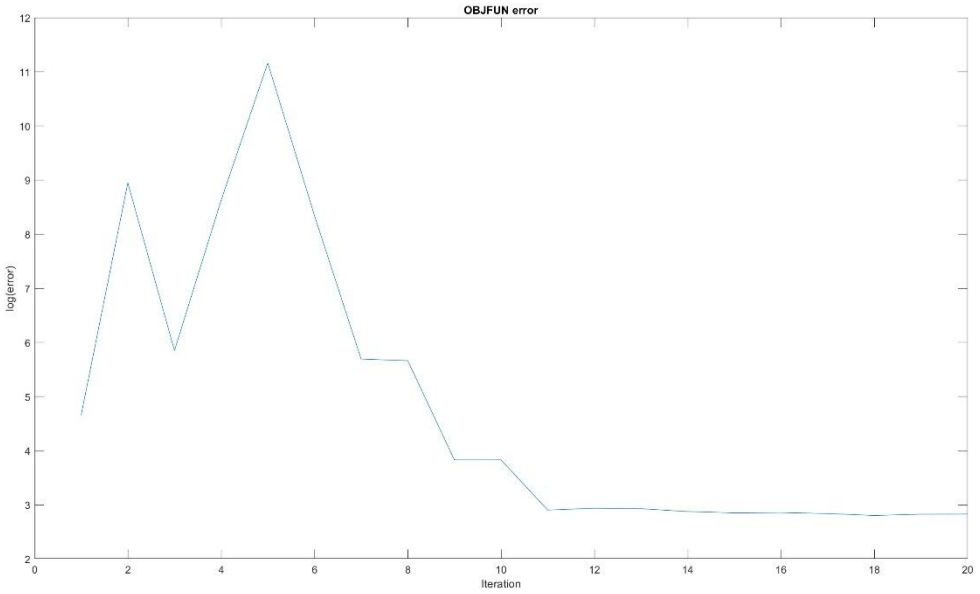

Figure 4.17 Evolution of the objective function during the NNO process.

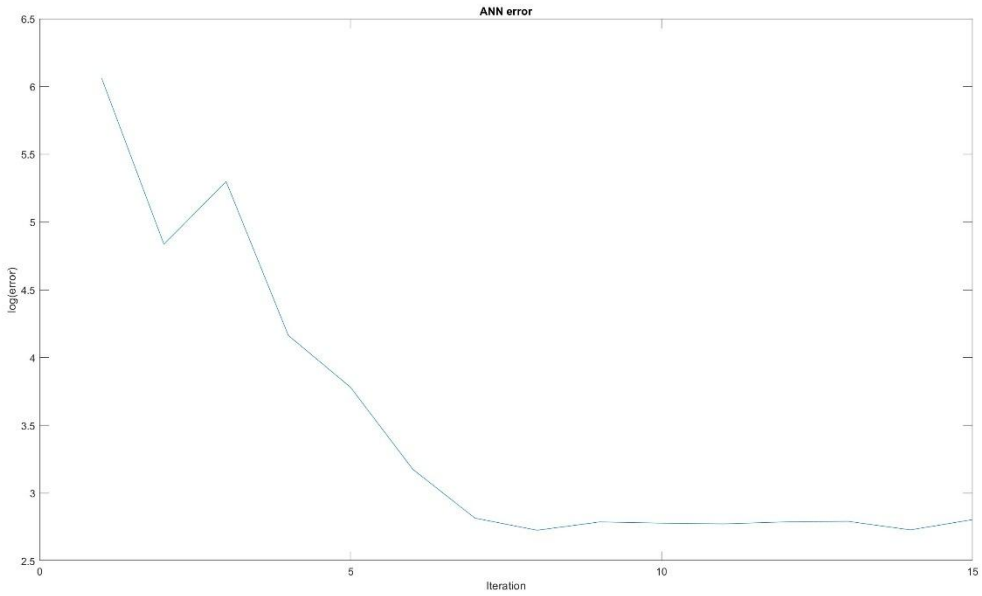

Figure 4.18 ANN error during optimization

One limitation of this approach is the use of simulated data as the optimization target. While it allows controlled benchmarking, real-world experimental data may include noise, bias, and unmodeled dynamics. Therefore, future validation with physical experiments is recommended to assess robustness in practice.

Additionally, the optimization space was bound narrowly around known values. In a real scenario with less prior knowledge, the search space would need to be broader, potentially increasing the number of simulations required.

These results validate the NNO framework as a viable and efficient technique for nonlinear parameter identification in dynamic systems. Its ability to closely approximate complex hysteretic behavior with limited simulation data makes it particularly suitable for computationally expensive systems such as finite element models of Stockbridge dampers.

5 Stockbridge Damper Modeling

A Stockbridge damper is a specifically designed mechanical device that functions as a tuned mass damper, primarily employed to suppress wind-induced vibrations, particularly aeolian vibrations, in overhead power lines and other slender structures. Its characteristic dumbbell shape is formed by two weights that are rigidly attached to the ends of a short, flexible cable, known as the messenger cable. This messenger cable is then clamped at its midpoint to the main overhead conductor. The primary application of Stockbridge dampers is in overhead power transmission and distribution lines, where they play a crucial role in mitigating the damaging effects of aeolian vibrations, thereby preventing fatigue failure and extending the lifespan of the conductors.

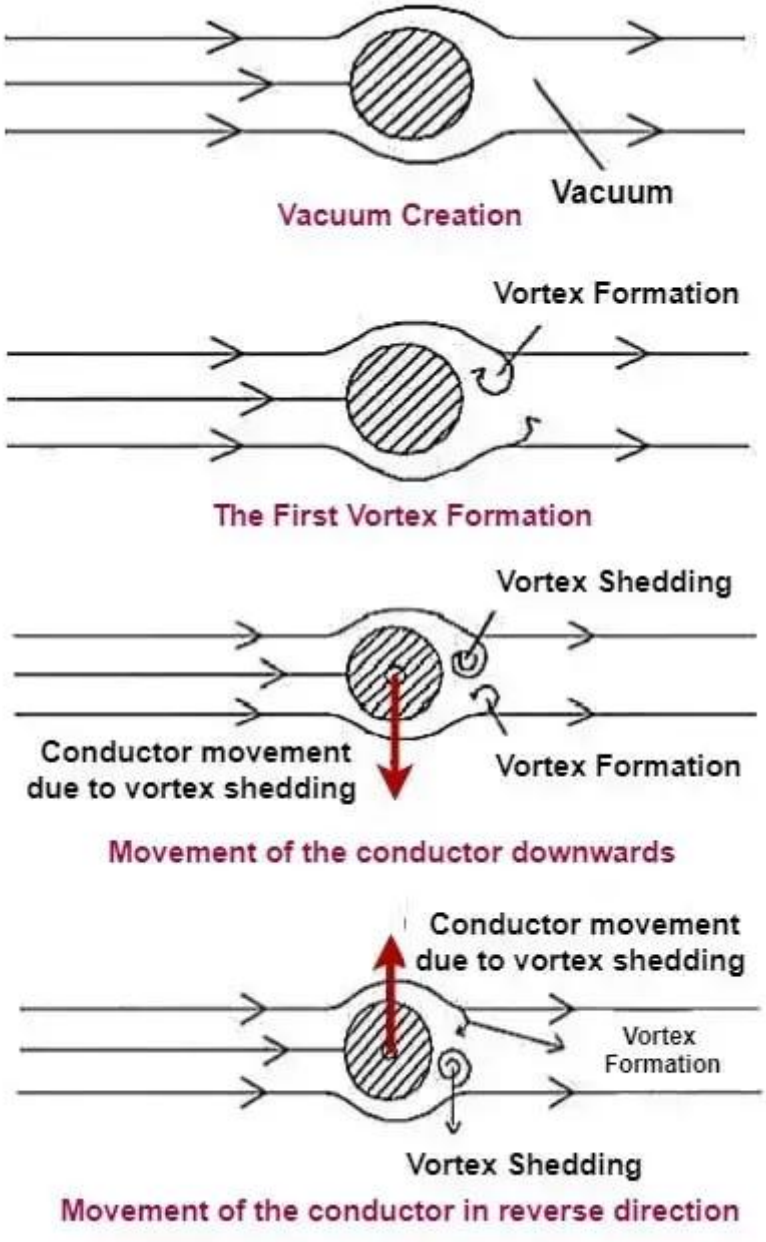

Figure 5.1 Aeolian Vibration

Beyond power lines, Stockbridge dampers find applications in other slender structures that are susceptible to wind-induced vibrations. These include cable-stayed bridges, where they help to dampen oscillations in the support cables; long cantilevered signs, preventing damage from wind-induced oscillations; radio mast guywires, where they reduce vibrations in the supporting cables; and even light poles, where they help prevent oscillations through resonance.

5.1 Geometry & Mechanics

The Stockbridge damper's effectiveness stems from its specific structural design and the interplay between its key components. These components include the messenger cable, the weights, and the clamp, each serving a distinct role in the vibration damping mechanism.

5.1.1 The Messenger Cable

The messenger cable is a crucial element of the Stockbridge damper, typically consisting of a short length of flexible, multi-stranded cable. The most common material for the messenger cable is galvanized steel, chosen for its high tensile strength, which allows it to withstand the bending stresses induced by vibrations, and its inherent flexibility, which enables the necessary oscillatory motion relative to the conductor. In environments with high levels of humidity or corrosive agents, some designs utilize stainless steel messenger cables for enhanced resistance to degradation. The primary function of the messenger cable is to connect the weights to the central clamp, facilitating their oscillatory movement in response to vibrations in the main conductor. The flexibility and stiffness characteristics of the messenger cable are critical design parameters, as they directly influence the resonant frequencies of the damper, allowing it to be tuned to effectively counteract specific vibration frequencies on the power line. A key aspect of the messenger cable's role in damping is the inter-strand friction that occurs within the multi-stranded construction as the cable flexes. This friction converts the mechanical energy of the vibration into heat, which is then dissipated into the environment, effectively reducing the amplitude of the oscillations. Furthermore, the length of the messenger cable is a significant factor in determining the damper's resonant frequencies, requiring careful consideration during the design process to ensure optimal performance.

5.1.2 The Weights

The Stockbridge damper features two weights that are attached to the ends of the messenger cable. These weights play a critical role by providing inertia to the damper system and by contributing to the creation of resonant frequencies that are designed to counteract the vibrations in the overhead conductor. The design of the weights has evolved significantly since the initial invention of the Stockbridge damper, which utilized concrete blocks as the inertial masses. Modern dampers typically employ metal weights made from materials such as galvanized steel, cast iron, or aluminum. These materials offer improved durability and performance compared to concrete. The shape of the weights has also undergone refinement. Many modern designs feature bell-shaped weights, which are often hollow and allow for some relative motion between the weight and the messenger cable. Some of these bell-shaped weights incorporate an asymmetric mass distribution, enabling the damper to oscillate in multiple frequency modes and ranges, thus providing more effective damping across a broader spectrum of aeolian vibration frequencies.

5.1.3 The Clamp

The clamp is the central component of the Stockbridge damper that provides a rigid connection between the messenger cable and the overhead conductor. It is typically manufactured from aluminum alloy due to its favorable strength-to-weight ratio and excellent resistance to corrosion, which is essential for long-term performance in outdoor installations. Depending on the manufacturer and specific design, the clamp may be produced using either forging or casting techniques. The most common method of attaching the clamp to the conductor involves a bolted mechanism, often utilizing galvanized steel bolts for their strength and corrosion resistance. Some designs also incorporate stainless steel safety plates for added security. To ensure that the clamp remains tightly secured to the conductor despite temperature fluctuations and current load cycling, aluminum clamping bolts are sometimes employed. For ease of installation and to ensure consistent clamping force, some Stockbridge dampers are equipped with breakaway bolts, which are designed to shear off at a predetermined torque level, eliminating the need for specialized torque wrenches. A secure and reliable grip of the clamp on the conductor is paramount, as it ensures efficient transfer of vibrations from the conductor to the damper's messenger cable and weights. In addition to bolted clamps, some manufacturers offer Stockbridge dampers with helical rod attachments as an alternative method for securing the damper to the conductor.

5.2 Finite Element Model

The previous work on Stockbridge dampers elaborates on the development of a finite element model (FEM) for the Stockbridge damper, a crucial component in mitigating vibrations in overhead power lines. The FEM provides a mathematical representation of the damper's dynamic behavior, enabling accurate analysis and prediction of its response to various forces and conditions.

The FEM development has been previously done by [29].

The model is constructed using a systematic procedure, which can be broken down into the following key steps:

- Identification of Inertial and Stiffness Contributions: This initial step involves a thorough definition of all the parameters that govern the dynamic behavior of the Stockbridge damper. These parameters encompass both inertial properties (related to mass and its distribution) and stiffness properties (related to the damper's resistance to deformation).
- Distribution of Inertial and Stiffness Properties with Shape Functions: Once the parameters are identified, their inertial and stiffness characteristics must be assigned throughout the model. This is achieved using shape functions, which are mathematical functions that describe how displacement varies within each element of the finite element mesh. These shape functions allow for the approximation of continuous displacement fields using discrete element values. The properties are initially defined in a local coordinate frame specific to each element.
- Projection (Rotation) of Local Matrices into Global Reference Frame: Finite element analysis involves multiple coordinate systems. The element-level matrices, formulated in local coordinate systems, need to be transformed into a common global reference frame. This transformation, often involving rotation matrices, ensures that all element

matrices are expressed in a consistent coordinate system before they can be assembled. However, in this case, since the local and global reference frames are aligned (horizontal), the rotation matrix becomes an identity matrix, simplifying the transformation.

- Assembly: The final step involves combining the individual element matrices (mass and stiffness) into a single global matrix representing the entire Stockbridge damper system. This assembly process follows specific rules based on the connectivity of the elements, resulting in a larger matrix that captures the overall dynamic behavior of the structure.

5.2.1 Scheme of the Damper (FEM)

The Stockbridge damper is modeled as a simplified system consisting of a three-node Euler-Bernoulli beam. This beam represents the messenger cable, and it is connected to lumped masses (representing the end masses and the clamp) through rigid links. To simplify the analysis, the motion is assumed to be constrained to the vertical plane, neglecting any horizontal displacement. Consequently, each node in the model possesses two degrees of freedom (2DOF): vertical displacement and rotation. This representation results in a 6-DOF system for the Stockbridge damper.

- x_1, x_c, and x_2 represent the vertical displacements of the nodes.
- φ_1, φ_c, and φ_2 represent the rotational displacements of the nodes.

The dynamic behavior of the Stockbridge damper is governed by several key parameters:

- m_1 and m_2: The masses of the end weights.
- m_c: The mass of the clamp.
- μ: The linear density of the messenger cable (kg/m).
- J_{G1} and J_{G2}: The moments of inertia of the end masses about their respective centers of mass.
- J_{GC}: The moment of inertia of the clamp about its center of mass.
- EI: The flexural rigidity of the messenger wire (Nm²). This is the product of the Young's modulus (E, in N/m²) and the area moment of inertia (I, in m⁴) of the wire's cross-section.
- a_1, a_2, and a_c:: The distances between the rotation axis and the center of mass of the end masses and the clamp, respectively.
- L_1 and L_2: The free lengths of the messenger cable between the clamp and the attachment points of the end masses.

5.2.2 Final Matrices

After the FEM development [29] the mass and stiffness matrices for each element are as below:

$$[M_{wire,e1}] = \frac{\mu l_{e1}}{420}\begin{bmatrix} 156 & 22l_{e1} & 54 & -13l_{e1} & 0 & 0 \\ 22l_{e1} & 4l_{e1}^2 & 13l_{e1} & -3l_{e1}^2 & 0 & 0 \\ 54 & 13l_{e1} & 156 & -22l_{e1} & 0 & 0 \\ -13l_{e1} & -3l_{e1}^2 & -22l_{e1} & 4l_{e1}^2 & 0 & 0 \\ 0 & 0 & 0 & 0 & 0 & 0 \\ 0 & 0 & 0 & 0 & 0 & 0 \end{bmatrix}$$

$$[M_{Lump,e1}] = \begin{bmatrix} m_1 & m_1 a_1 & & \cdots & & 0 \\ m_1 a_1 & J_{G1} + m_1 a_1^2 & & & & \\ & & m_c & m_c a_c & & \\ \vdots & & m_c a_c & J_{GC} + m_c a_c^2 & \vdots & \\ & & & & 0 & 0 \\ 0 & & \cdots & & 0 & 0 \end{bmatrix}$$

$$[M_1] = [M_{wire,e1}] + [M_{Lump,e1}]$$

$$[M_{wire,e2}] = \frac{\mu l_{e2}}{420} \begin{bmatrix} 0 & 0 & 0 & 0 & 0 & 0 \\ 0 & 0 & 0 & 0 & 0 & 0 \\ 0 & 0 & 156 & 22l_{e2} & 54 & -13l_{e2} \\ 0 & 0 & 22l_{e2} & 4l_{e2}^2 & 13l_{e2} & -3l_{e2}^2 \\ 0 & 0 & 54 & 13l_{e2} & 156 & -22l_{e2} \\ 0 & 0 & -13l_{e2} & -3l_{e2}^2 & -22l_{e2} & 4l_{e2}^2 \end{bmatrix}$$

$$[M_{Lump,e1}] = \begin{bmatrix} 0 & 0 & \cdots & & 0 \\ 0 & 0 & & & \\ \vdots & & 0 & 0 & \vdots \\ & & 0 & 0 & \\ 0 & \cdots & & m_2 & m_2 a_2 \\ & & & m_2 a_2 & J_{G2} + m_2 a_2^2 \end{bmatrix}$$

$$[M_2] = [M_{wire,e2}] + [M_{Lump,e2}]$$

$$[K_{wire,e1}] = EI \begin{bmatrix} 12/l_{e1}^3 & 6/l_{e1}^2 & -12/l_{e1}^3 & 6/l_{e1}^2 & 0 & 0 \\ 6/l_{e1}^2 & 4/l_{e1} & -6/l_{e1}^2 & 2/l_{e1} & 0 & 0 \\ -12/l_{e1}^3 & -6/l_{e1}^2 & 12/l_{e1}^3 & -6/l_{e1}^2 & 0 & 0 \\ 6/l_{e1}^2 & 2/l_{e1} & -6/l_{e1}^2 & 4l_{e1} & 0 & 0 \\ 0 & 0 & 0 & 0 & 0 & 0 \\ 0 & 0 & 0 & 0 & 0 & 0 \end{bmatrix}$$

$$[K_{wire,e2}] = EI \begin{bmatrix} 0 & 0 & 0 & 0 & 0 & 0 \\ 0 & 0 & 0 & 0 & 0 & 0 \\ 0 & 0 & 12/l_{e2}^3 & 6/l_{e2}^2 & -12/l_{e2}^3 & 6/l_{e2}^2 \\ 0 & 0 & 6/l_{e2}^2 & 4/l_{e2} & -6/l_{e2}^2 & 2/l_{e2} \\ 0 & 0 & -12/l_{e2}^3 & -6/l_{e2}^2 & 12/l_{e2}^3 & -6/l_{e2}^2 \\ 0 & 0 & 6/l_{e2}^2 & 2/l_{e2} & -6/l_{e2}^2 & 4l_{e2} \end{bmatrix}$$

$$[K] = [K_{wire,e1}] + [K_{wire,e2}]$$

5.3 Equations of Motion and Adapting Bouc-Wen to Stockbridge Dampers

After testing the Bouc-Wen damping and Cubic Stiffness and Newmark Integration method and NNO on SDOF and MDOF systems we Move on the initial problem of modeling of the Stockbridge damper.

The dynamic behavior of a Stockbridge damper can be modeled using second-order nonlinear differential equations, capturing both the linear and nonlinear forces acting on the system. These forces arise from mass inertia, linear elastic and damping characteristics, and nonlinear hysteretic and geometric effects. The generalized equation of motion is given by:

$$M\,\ddot{y}(t) + r(y,\dot{y}) + F_{NL}(y,\dot{y}) = u(t)$$

where M is the mass matrix, $y(t)$ is the displacement vector, $\dot{y}(t)$ and $\ddot{y}(t)$ represent velocity and acceleration respectively, $r(y,\dot{y})$ is the linear restoring force, $F_{NL}(y,\dot{y})$ is the nonlinear force contribution, and $u(t)$ is the external excitation (e.g., wind-induced vibration or cable motion).

The linear restoring force is composed of both elastic and viscous terms:

$$r(y,\dot{y}) = K\,y + C\,\dot{y}$$

where is the stiffness matrix K and C is the damping matrix. These account for the standard linear spring-damper behavior of the damper arms.

To capture the nonlinear behavior, particularly the complex hysteresis observed in Stockbridge dampers, a combination of geometric and hysteretic nonlinear forces is included:

$$F_{NL}(y,\dot{y}) = F_{BW}(y,\dot{y}) + F_{CS}(y)$$

Here, $F_{CS}(y)$ represents a cubic stiffness component introduced to account for geometric nonlinearities and stiffness hardening/softening effects:

$$F_{CS}(y) = K_{CS}\,y(t)^3$$

where K_{CS} is a nonlinear stiffness coefficient.

The term $F_{Bw}(y,\dot{y})$ incorporates hysteretic behavior via the Bouc-Wen model[25], [26], which is widely used to describe the rate-independent hysteresis in mechanical systems:

$$F_{Bw}(y,\dot{y}) = \alpha\,y(t) + (1-\alpha)\,D\,z(t)$$

In this formulation, α is a weighting factor between the linear and hysteretic contributions, D is a scaling parameter, and $z(t)$ is the internal hysteretic variable governed by the Bouc-Wen differential equation:

$$\dot{z} = D^{-1}(A\,\dot{x} - \beta|\dot{x}||z|^{\nu-1}\,z\; -\; \gamma\,\dot{x}|z|^{\nu})$$

The parameters A, β, γ, and ν control the shape and behavior of the hysteresis loop. Specifically:

- A defines the linear contribution to the rate of change of z
- β and γ control the nonlinear interaction between the velocity and the hysteretic force,
- ν shapes the smoothness or sharpness of the hysteretic transition.

This formulation allows the model to adapt to the energy dissipation and memory-dependent behavior observed in experimental Stockbridge damper responses, making it suitable for accurate simulation and design optimization.

5.4 Experimental Data

The prototype is tested on an electromagnetic shaker. Its clamp is fixed on the base of the shaker at the prescribed tightening torque. The test consists of feeding an excitation profile to the device (i.e., the shaker base) in terms of amplitude over a specific range of frequencies. The shaker is governed in closed loops by a certified control software and the adopted sensors are all calibrated: the entire test bench is called DTS (Damper testing system). The logged signals are post processed by the same software that can produce many types of diagrams like dynamic stiffness, power dissipation, and impedance.

The displacement of the clamp is logged thanks to an accelerometer solid with the shaker base. The damper's response in terms of force is logged with two load cells.

The following experimental data are extracted from [29].

The acquired experimental data are in the case of sweep up excitation, and the displacements of the base and both masses have been measured and are in Figure 5.2.

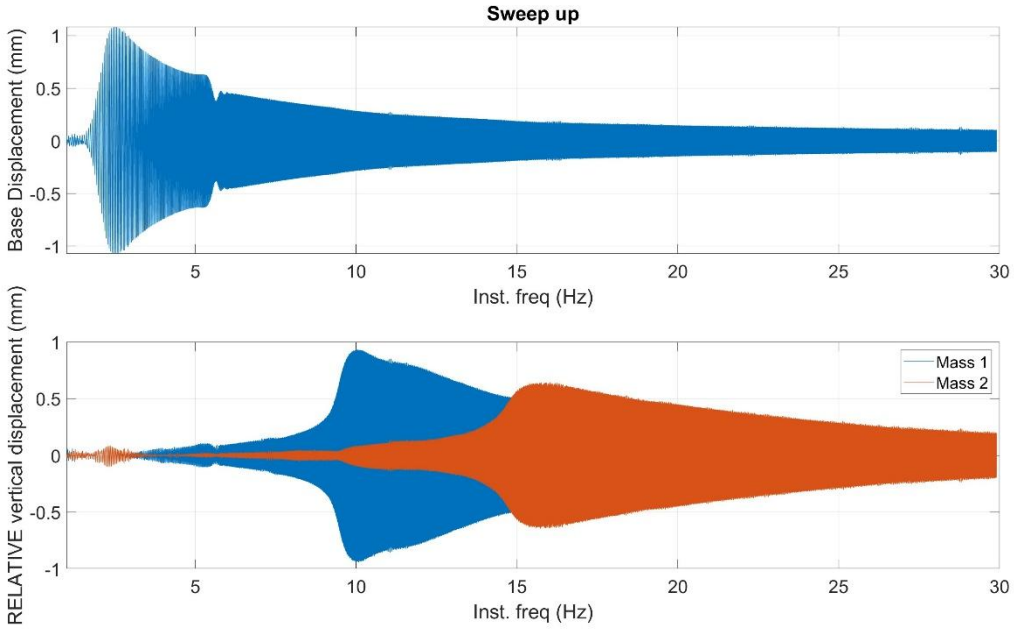

Figure 5.2 Sweep up input and output displacements of the mass 1 and 2

Figure 5.3 illustrates the PSDs of both masses which are being used to optimize the nonlinear model.

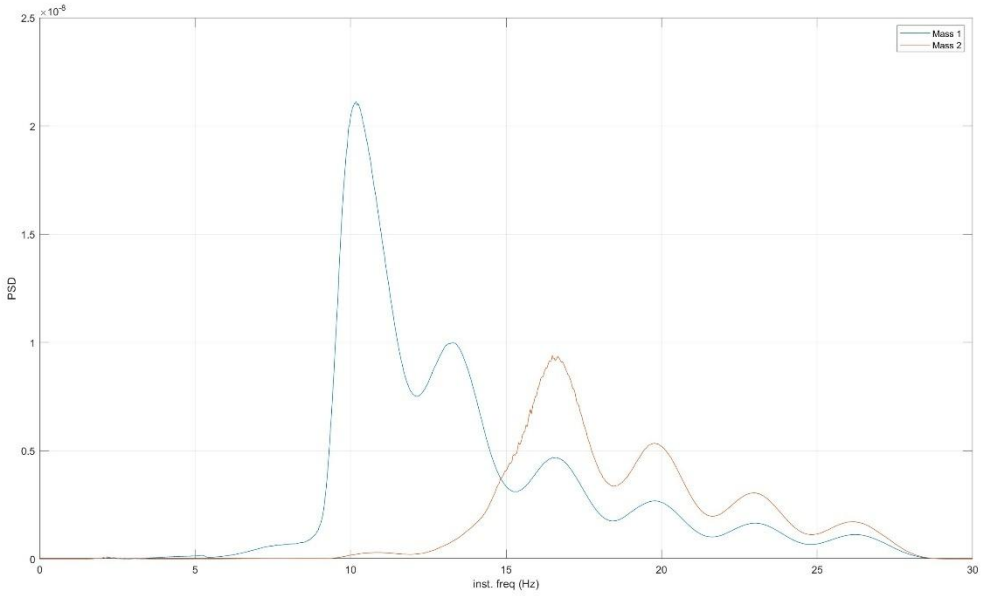

Figure 5.3 PSD of end masses of Stockbridge damper

Figure 5.4 and Figure 5.5 are representations of input-output characteristics, and displacement-velocity of the masses in the peak frequencies of the displacement shown in Figure 5.2.

Figure 5.4 Hysteresis loop in the system input-output plane at 10 Hz

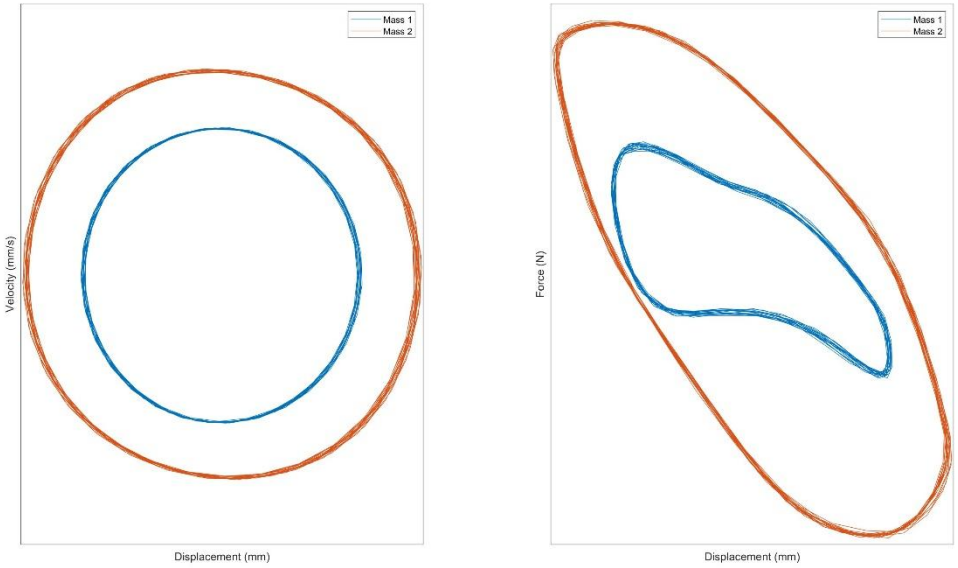

Figure 5.5 Hysteresis loop in the system input-output plane at 17 Hz

5.5 Results of Optimization

The optimization process was carried out in four distinct stages, using Power Spectral Density (PSD) as the performance metric to guide and evaluate the results. PSD analysis allowed us to quantify the vibrational response of the system across a range of frequencies, making it a suitable objective function for optimizing dynamic performance. We began by optimizing a single mass parameter at a time—first one, then the other—while keeping the rest of the configuration fixed. This helped isolate the influence of each mass on the system's frequency response. After optimizing the masses individually, we performed joint optimization on both masses simultaneously to capture any interaction effects. This stage was repeated several times to ensure stability and repeatability of the solutions. Finally, to benchmark the effectiveness of our Neural Network Optimization (NNO) method, we applied a Genetic Algorithm (GA) to the same problem and compared the results. The comparison provided valuable insight into the relative strengths of each optimization technique, especially in terms of how effectively they minimized the PSD across the frequency range of interest.

5.5.1 Optimization of Mass 1

To carry out the optimization of mass 1, a total of eight parameters were considered. These parameters, listed in the Table 5.1, were selected based on their influence on the dynamic behavior of the system and their relevance to the vibrational response captured through Power Spectral Density (PSD). Each parameter plays a specific role, either directly affecting the mass properties or indirectly shaping the system's frequency response characteristics. By tuning these parameters, we aimed to minimize the PSD within a target frequency range, thereby improving the system's performance under dynamic loading conditions.

Parameters	Definition	Lower bound	Upper bound
A	Bouc-Wen parameter[1]	1	10
β	Bouc-Wen parameter	0.1	5
γ	Bouc-Wen parameter	0	2
α	Bouc-Wen parameter	0	1
$EmJm$	Flexural stiffness	8	20
$k\_cs(1)$	Cubic stiffness	-5e9	-0.1e9
α_pd	Proportional damping coefficient	5	20
β_pd	Proportional damping coefficient	1e-3	10e-3

Table 5.1 Design parameters

[1] Nondimensional parameters, which control the shape and the size of the hysteresis loop

The NNO parameters are mentioned in Table 5.2.

Parameters	Definition	Value
nVar	Number of design variables	8
initSim	Number of Abaqus analyses for initial training of the neural network	15
hiddenSizes	Number and size of hidden layers	8
Psize	Population size	25
funTol	Termination tolerance of error between target and simulated curve	0.001
maxSim	Maximum number of iterations	60
XTol	Stall tolerance for X	0.04
YTol	Stall tolerance for Y	0.05

Table 5.2 NNO parameters

For mass 1 we get the following results after optimization:

Parameters	Optimized value
A	4.9371
β	3.9989
γ	1.1511
α	0.5895
$EmJm$	14.8458
$k\_cs(1)$	-2.9384 e9
α_pd	5.187
β_pd	1.6875 e-3

Table 5.3 Optimized results of mass 1

The results of the optimization of mass 1 are shown in Figure 5.6, and its comparison with experimental data is shown in Figure 5.7. As clearly visible, we have successfully replicated the vibration of mass 1 with very high accuracy, however the model is unable to replicate mass 2 accurately and the results are off by a high margin.

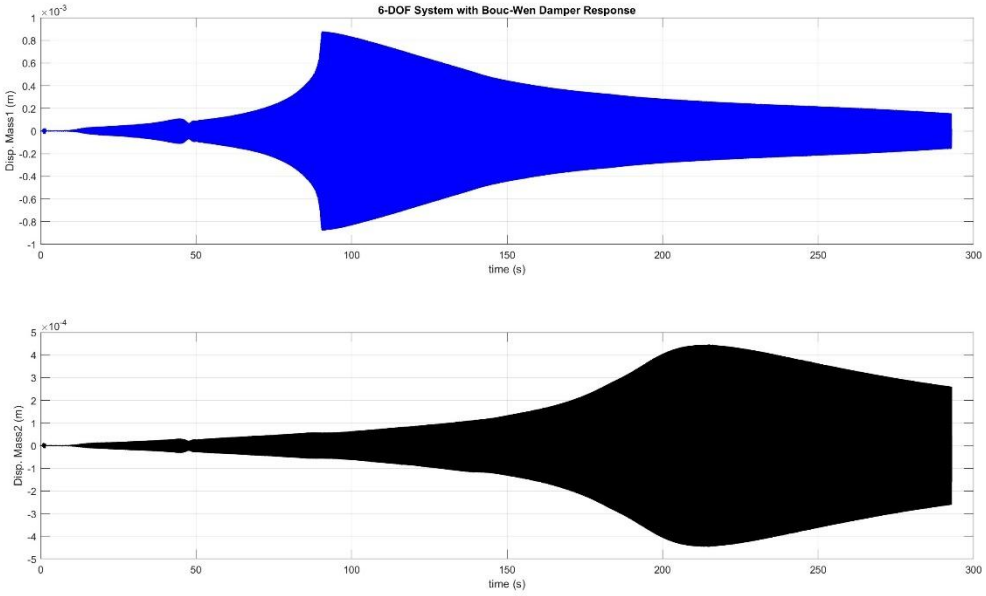

Figure 5.6 Displacements of mass 1 (blue) and mass 2 (black) after optimization

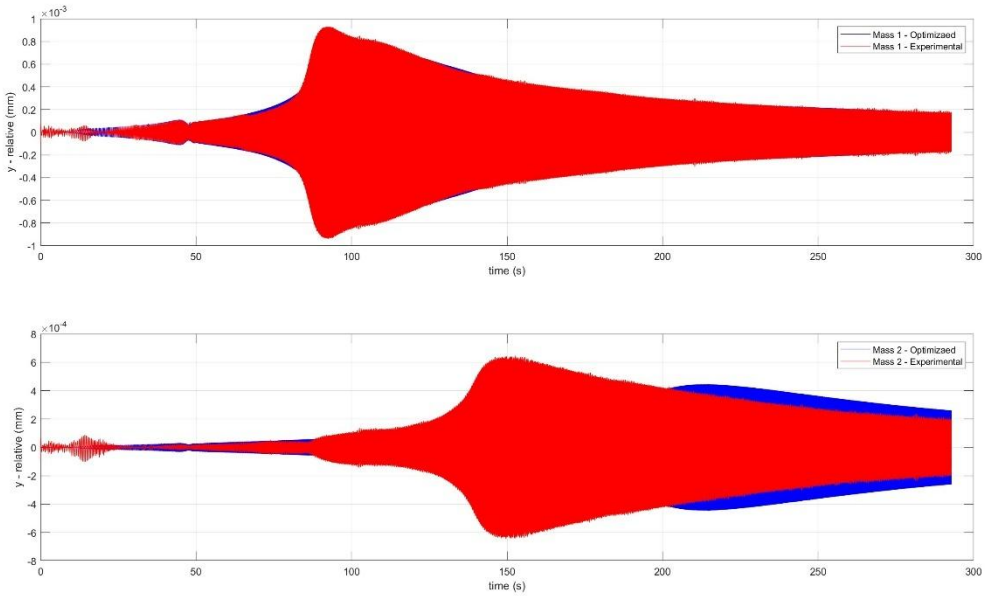

Figure 5.7 Comparison of the displacements of experimental data (red) and optimized data (blue)

As previously mentioned, the optimization has been carried out by using the vector of PSDs as our cost function. However, as the error vectors are very long and computationally heavy and not possible to work with, we only choose the most important part of the vector, which is the PSD between the frequencies of about 9 and 11.5 Hz.

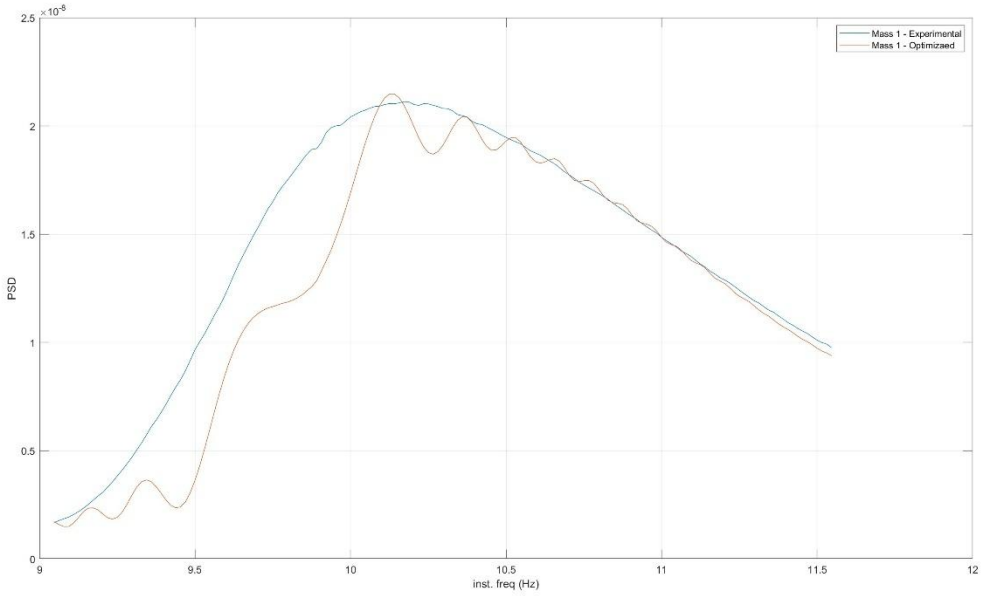

Figure 5.8 PSDs of experimental and optimized data in range of 9 to 11.5 Hz

Although we have used only the peak of the PSD to do the optimization, as is shown in Figure 5.9, the rest of the PSD excellently matches the experimental data. The error for mass one is approximately 3.28 percent.

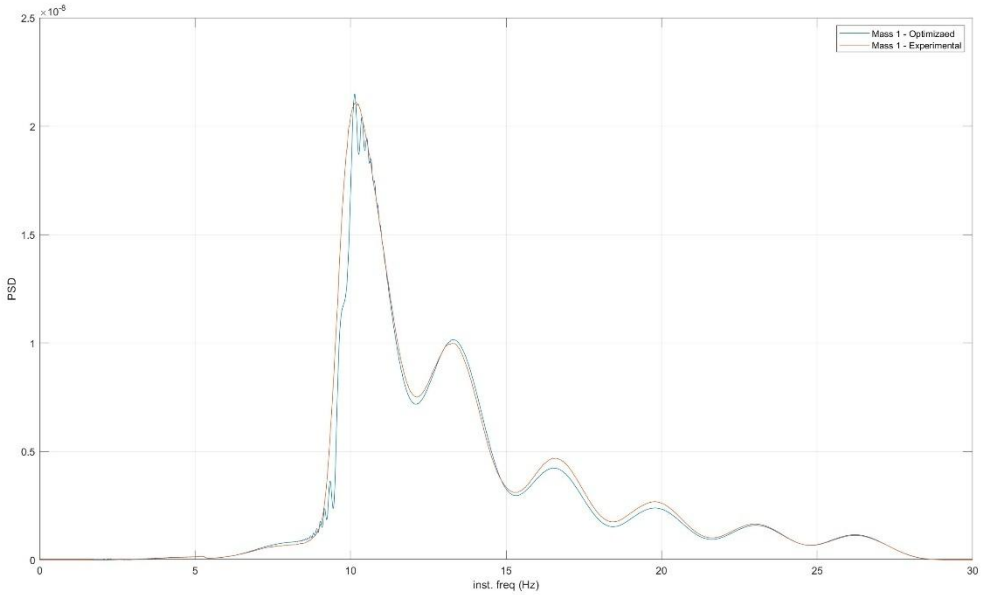

Figure 5.9 PSDs of experimental and optimized data of mass 1

5.5.2 Optimization of Mass 2

The same procedure has been done for mass 2. The only difference is the cubic stiffness argument that has been used. The parameters used are listed in the table.

Parameters	Definition	Lower bound	Upper bound
A	Bouc-Wen parameter	1	10
β	Bouc-Wen parameter	0.1	5
γ	Bouc-Wen parameter	0	2
α	Bouc-Wen parameter	0	1
$EmJm$	Flexural stiffness	8	20
$k\_cs(3)$	Cubic stiffness	-20e9	-3e9
α_pd	Proportional damping coefficient	5	20
β_pd	Proportional damping coefficient	1e-3	10e-3

Table 5.4 Design parameters

The optimization parameters are as mass 1, which are listed in the table.

At the end of the optimization, we get the following results:

Parameters	Optimized value
A	4.0824
β	0.3717
γ	1.674
α	0.9545
$EmJm$	8.2099
$k\_cs(3)$	-3.045 e9
α_pd	7.4522
β_pd	2.3011 e-3

Table 5.5 Optimized results of mass 2

This time we have been able to match the signal for mass 2 with the experimental data and in Figure 5.11 is shown that mass 1 vibrations are not close to the experimental data and we only can see the accuracy of results in mass 2.

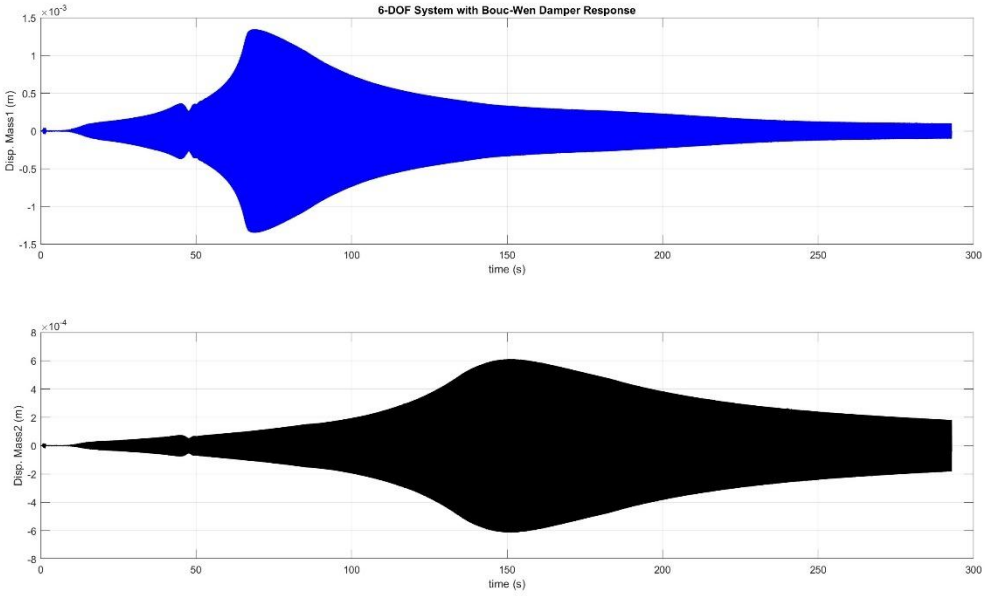

Figure 5.10 Displacements of mass 1 (blue) and mass 2 (black) after optimization

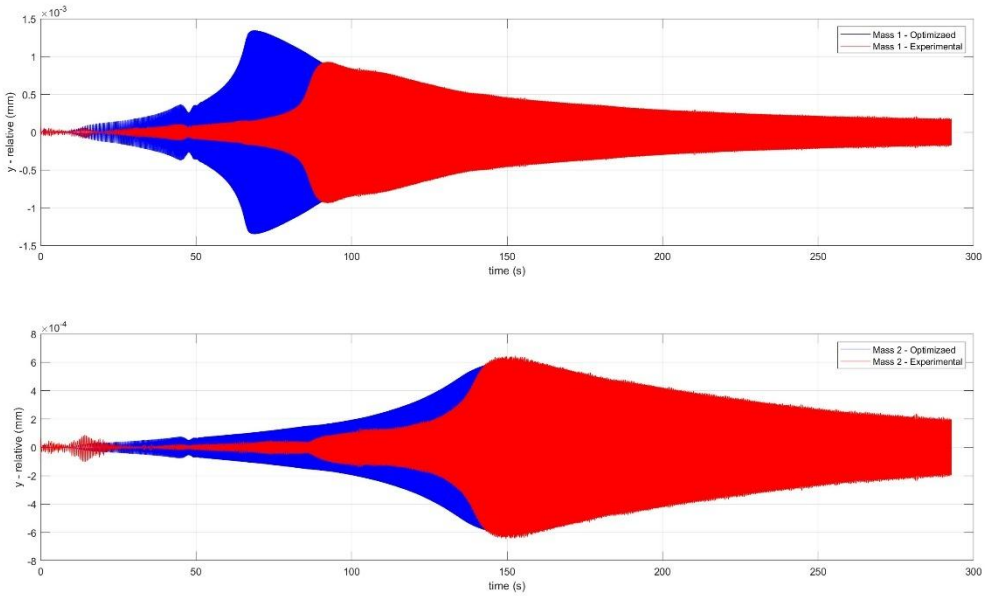

Figure 5.11 Comparison of the displacements of experimental data (red) and optimized data (blue)

In the case of mass 2, the range of the PSD that is being used is between 15.5 to 18 Hz (peak of the PSD). The error in the case of optimization of mass 2 is approximately 4.14 percent.

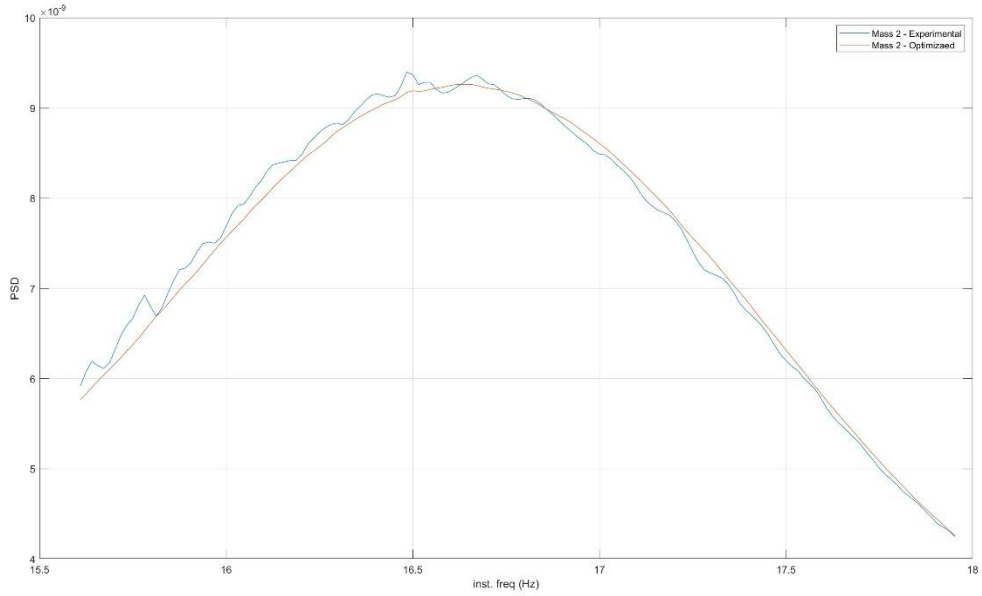

Figure 5.12 PSDs of experimental and optimized data in the range of 15.5 to 18 Hz

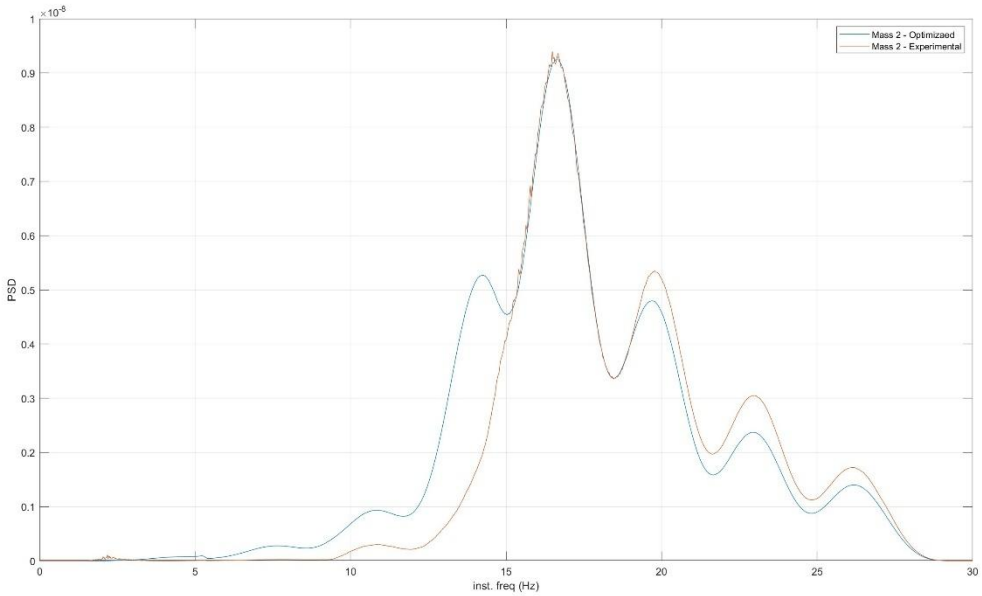

Figure 5.13 PSDs of experimental and optimized data of mass 2

5.5.3 Optimization of the Stockbridge Damper

In the third stage of the optimization, we try to optimize the whole system simultaneously. Design parameters and their boundaries are as mentioned in the Table 5.6.

Parameters	Definition	Lower bound	Upper bound
A	Bouc-Wen parameter	1	15
β	Bouc-Wen parameter	0.1	5
γ	Bouc-Wen parameter	-3	3
α	Bouc-Wen parameter	0	1
$EmJm$	Flexural stiffness	7	20
$k\_cs(1)$	Cubic stiffness	-2.5e9	-0.1e9
$k\_cs(2)$	Cubic stiffness	-18e9	-5e9
α_pd	Proportional damping coefficient	5	15
β_pd	Proportional damping coefficient	0.1 e-3	5 e-3

Table 5.6 Design parameters

The NNO parameters are mentioned in the Table 5.7.

Parameters	Definition	Value
nVar	Number of design variables	9
initSim	Number of Abaqus analyses for initial training of the neural network	18
hiddenSizes	Number and size of hidden layers	9
Psize	Population size	30
funTol	Termination tolerance of error between target and simulated curve	0.005
maxSim	Maximum number of iterations	60
XTol	Stall tolerance for X	0.05
YTol	Stall tolerance for Y	0.05

Table 5.7 NNO parameters

To be assured of reliability of the model and the optimization technique, the optimization has been done twice and the results of both are in Table 5.8.

Parameters	Results of optimization 1	Results of optimization 2
A	6.0	6.5771
β	1.1916	1.5162
γ	0.8677	1.5568
α	0.8406	0.6978
$EmJm$	10.0583	9.7385
$k\_cs(1)$	-0.25 e9	-0.4763 e9
$k\_cs(2)$	-13.1766 e9	-15.0288 e9
α_pd	9.9513	8.3236
β_pd	1.1026 e-3	1.0362 e-3

Table 5.8 Results of optimizations

The optimization errors in case 1 for mass 1 and mass 2 respectively are 4.4% and 1.4%. And in case 2 are 5.2% and 5.4% respectively.

The results of the optimization and their comparisons are in the figures.

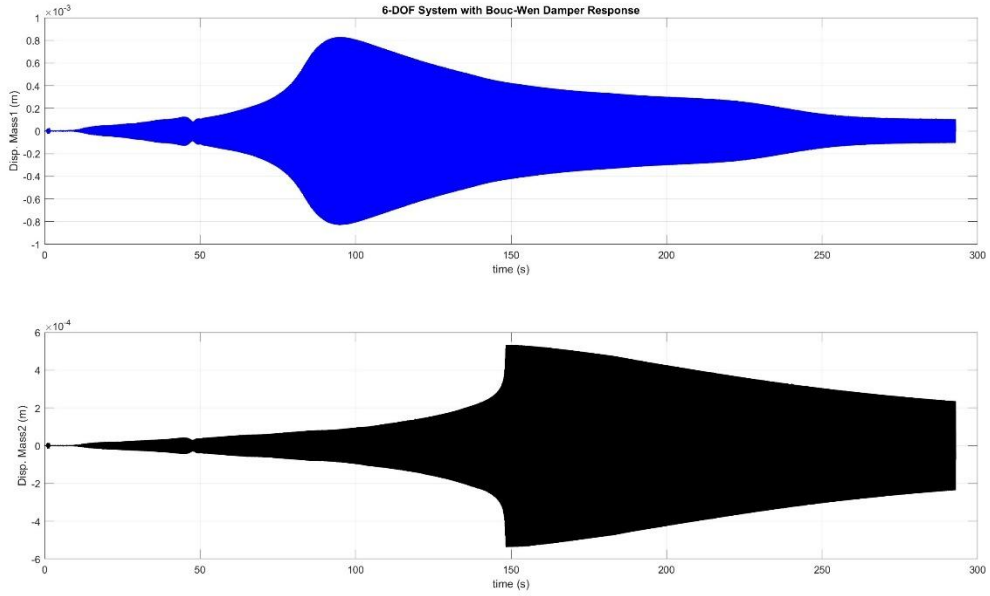

Figure 5.14 Displacements of the masses in Case 1

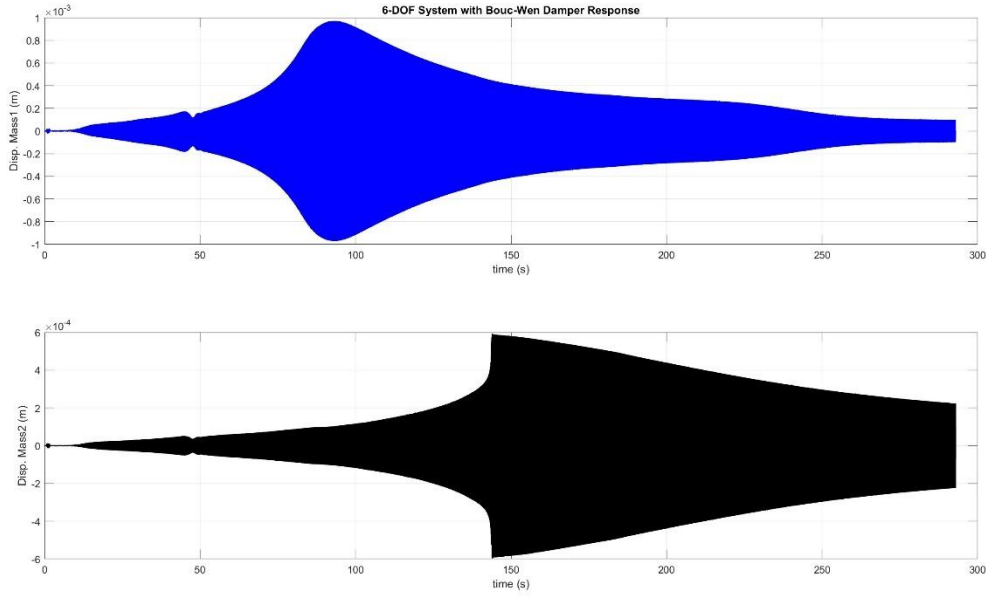

Figure 5.15 Displacements of the masses in Case 2

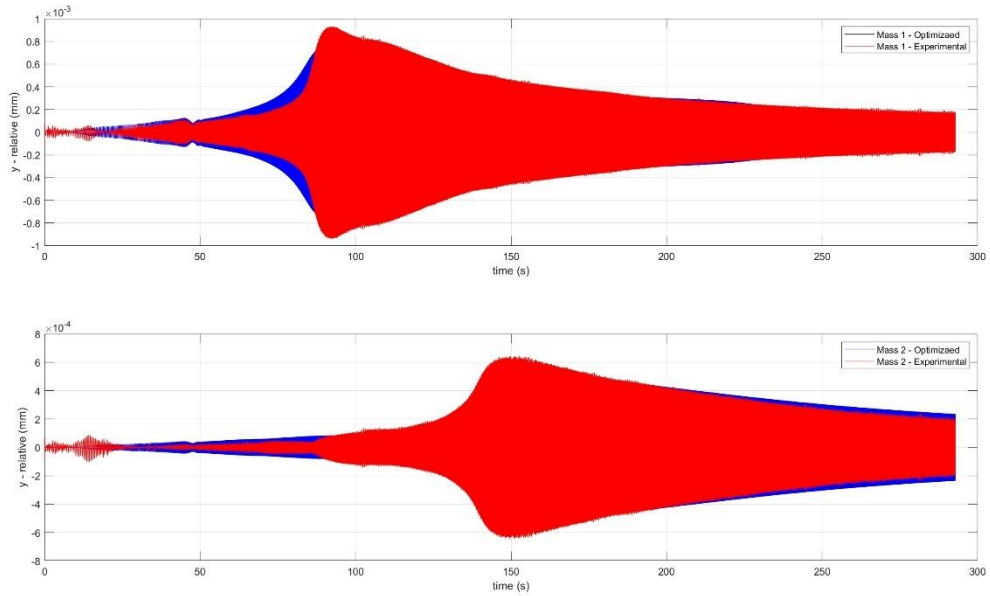

Figure 5.16 Comparison of Experimental and optimized data in Case 1

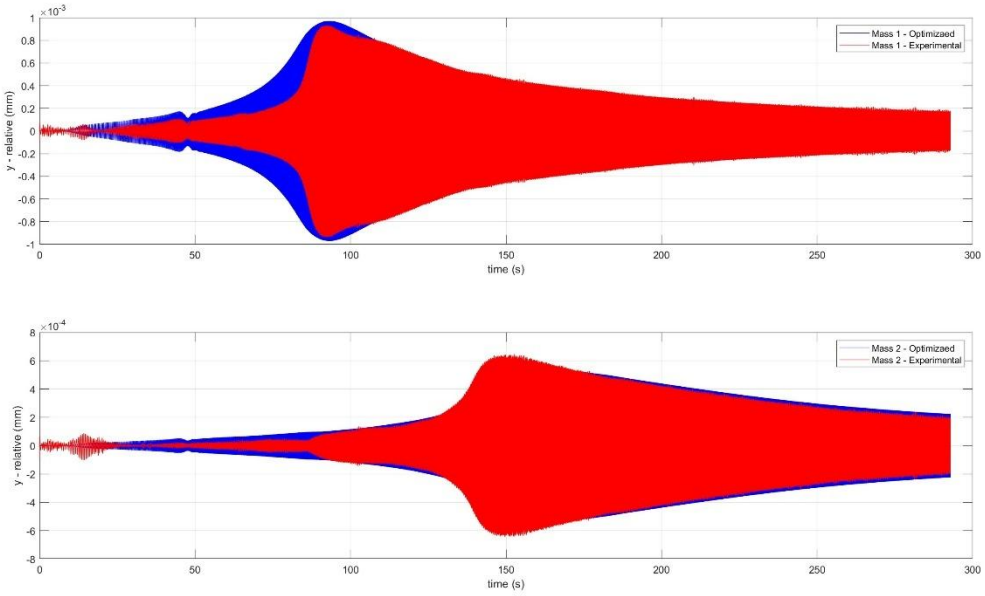

Figure 5.17 Comparison of Experimental and Optimized Data in Case 2

The range of PSDs that optimization has been carried on for mass 1 is approximately from 9 to 11.5 Hz and for mass 2 around 15.5 to 18 Hz.

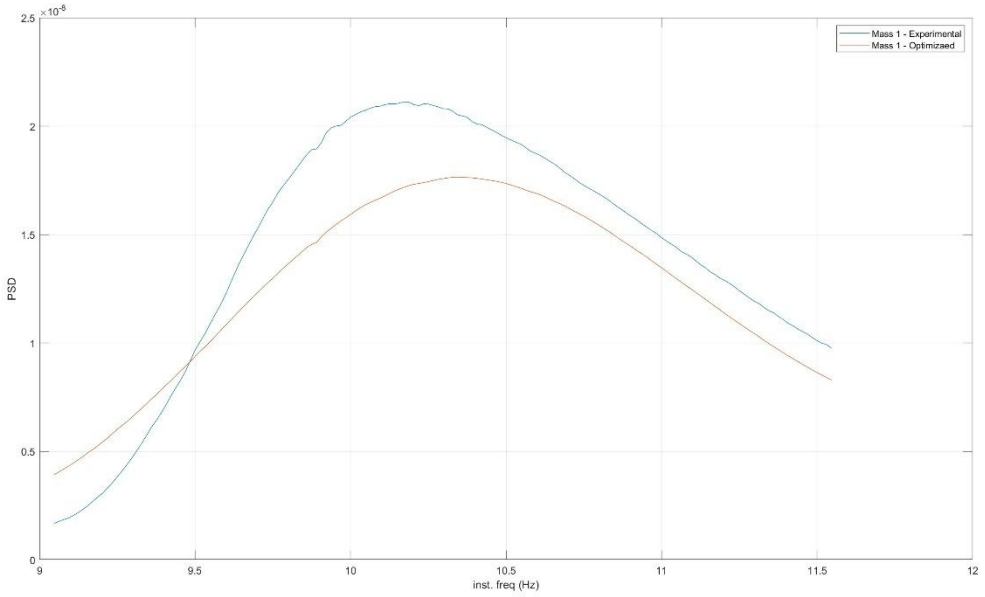

Figure 5.18 Peak of PSD of mass 1 in the range of 9 to 11.5 Hz in Case 1

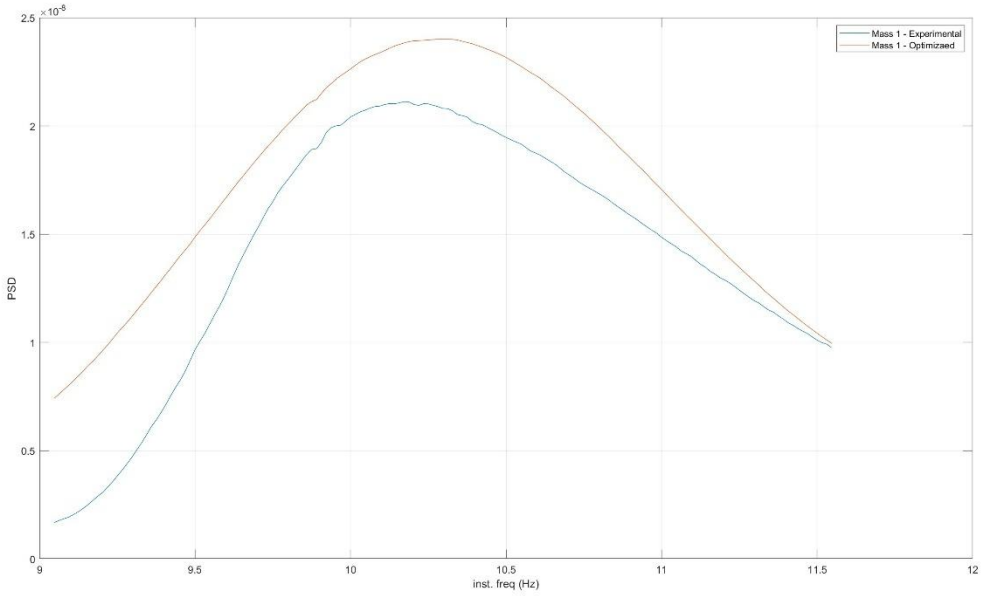

Figure 5.19 Peak of PSD of mass 1 in the range of 9 to 11.5 Hz in Case 2

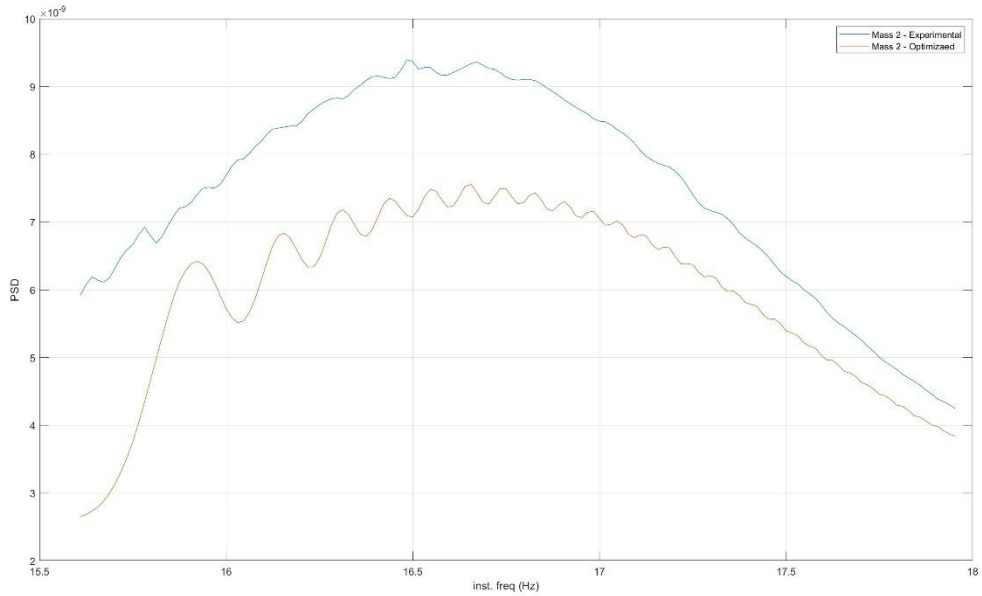

Figure 5.20 Peak of PSD of mass 2 in the range of 15.5 to 18 Hz in Case 1

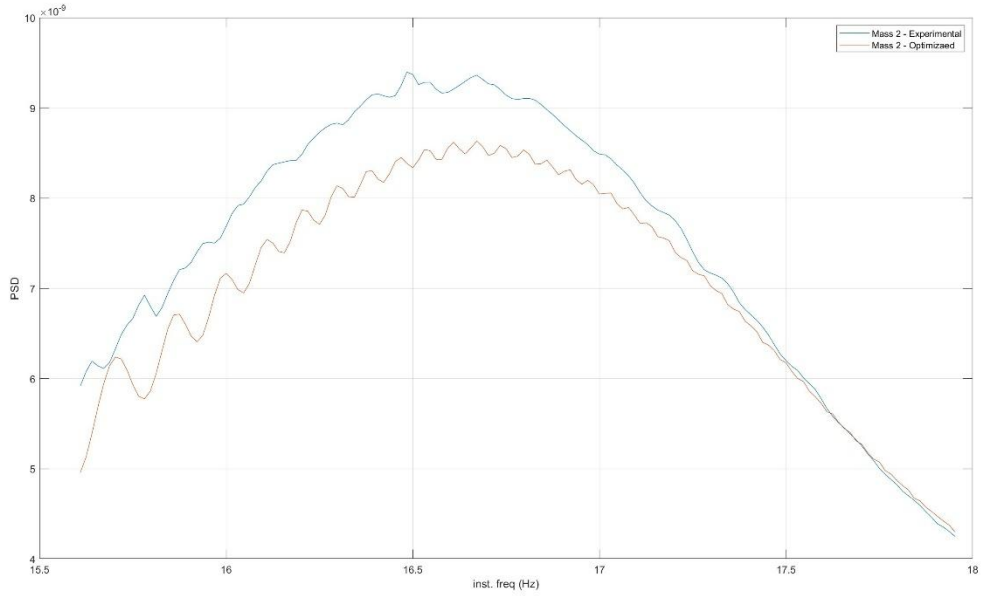

Figure 5.21 Peak of PSD of mass 2 in the range of 15.5 to 18 Hz in Case 2

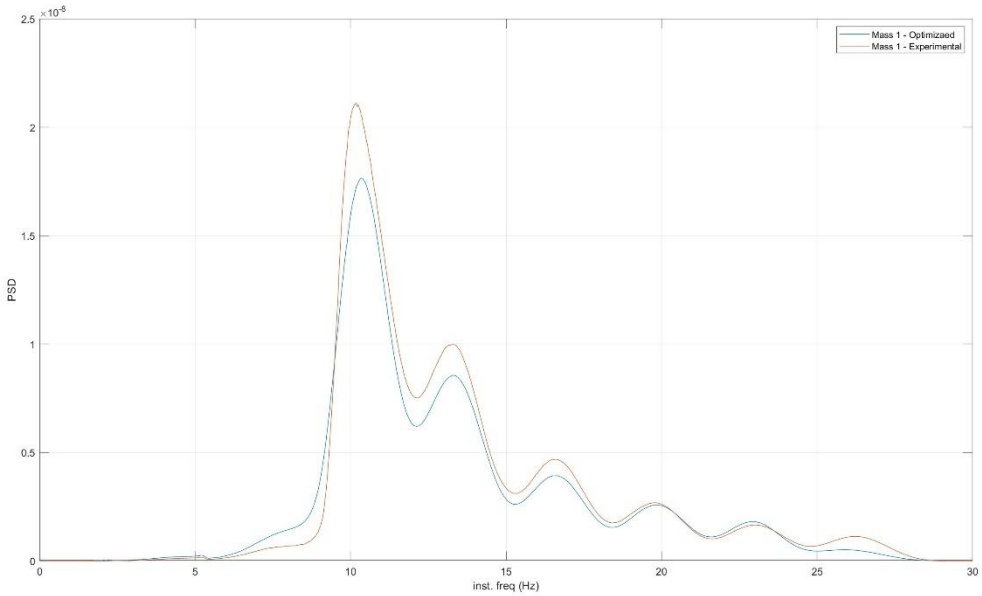

Figure 5.22 Experimental and optimized PSDs of mass 1 in Case 1

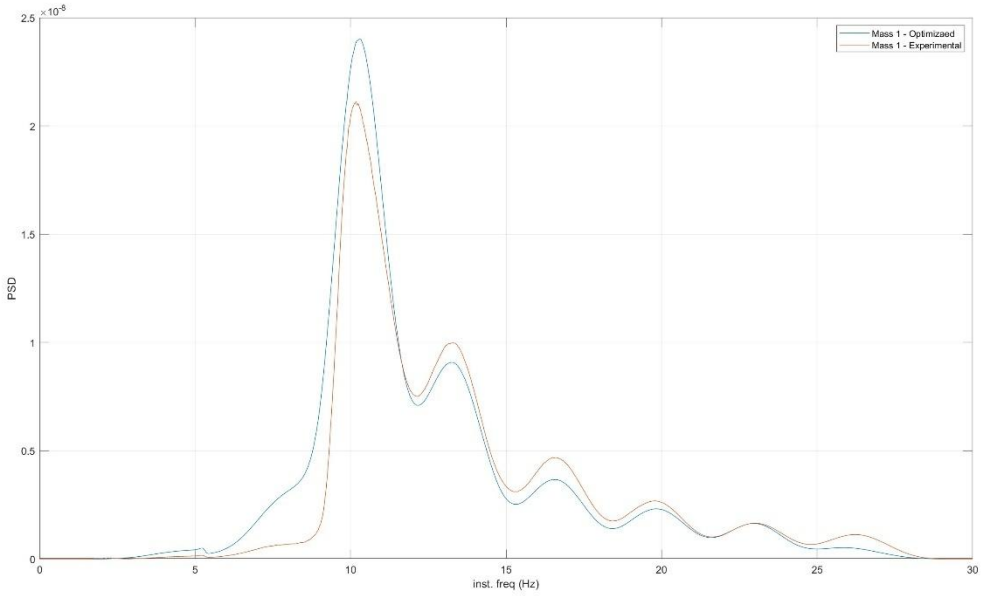

Figure 5.23 Experimental and optimized PSDs of mass 1 in Case 2

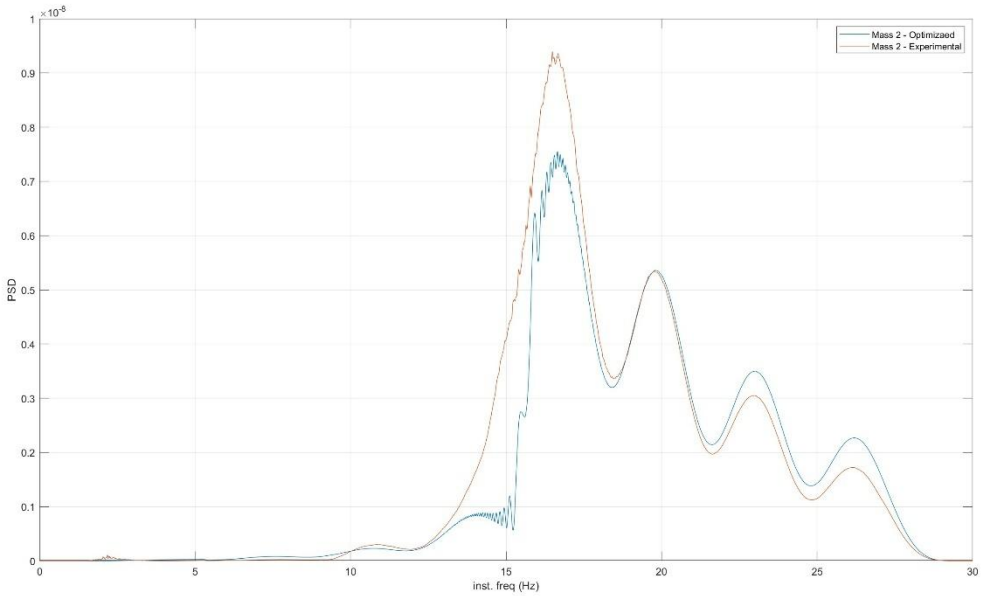

Figure 5.24 Experimental and optimized PSDs of mass 2 in Case 1

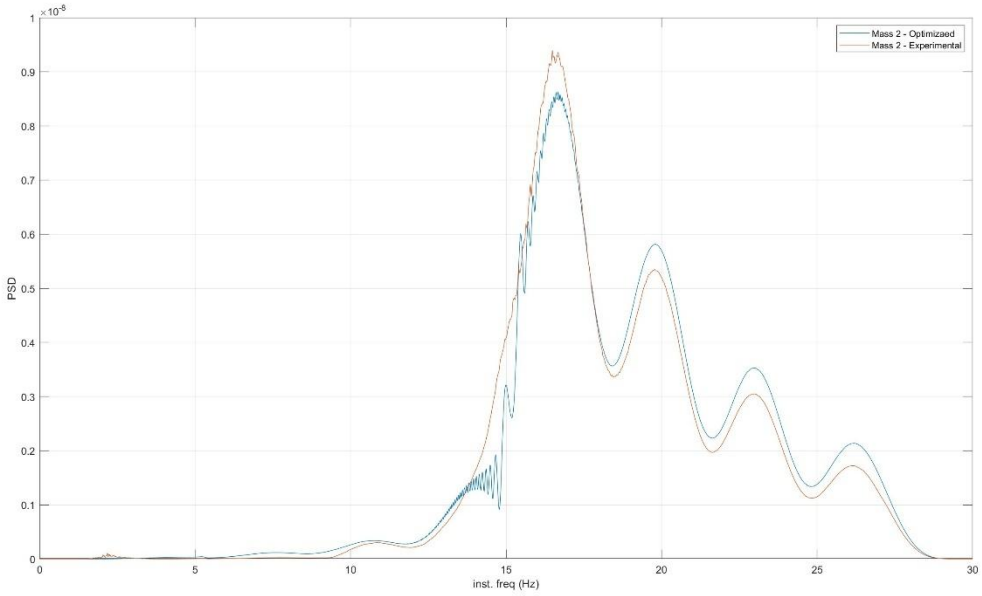

Figure 5.25 Experimental and optimized PSDs of mass 2 in Case 2

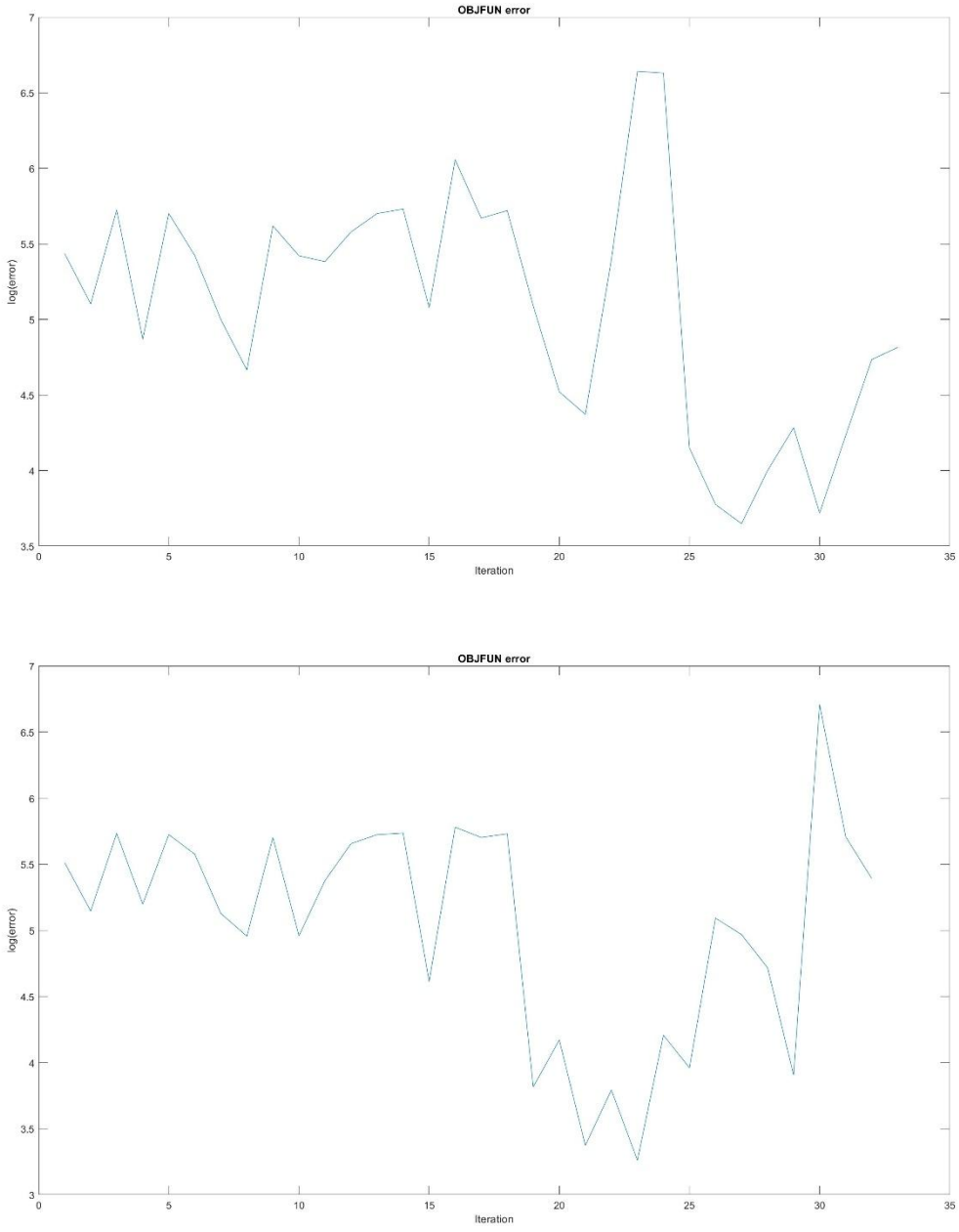

Figure 5.26 Objective function errors, Top: case 1, Bottom: case 2

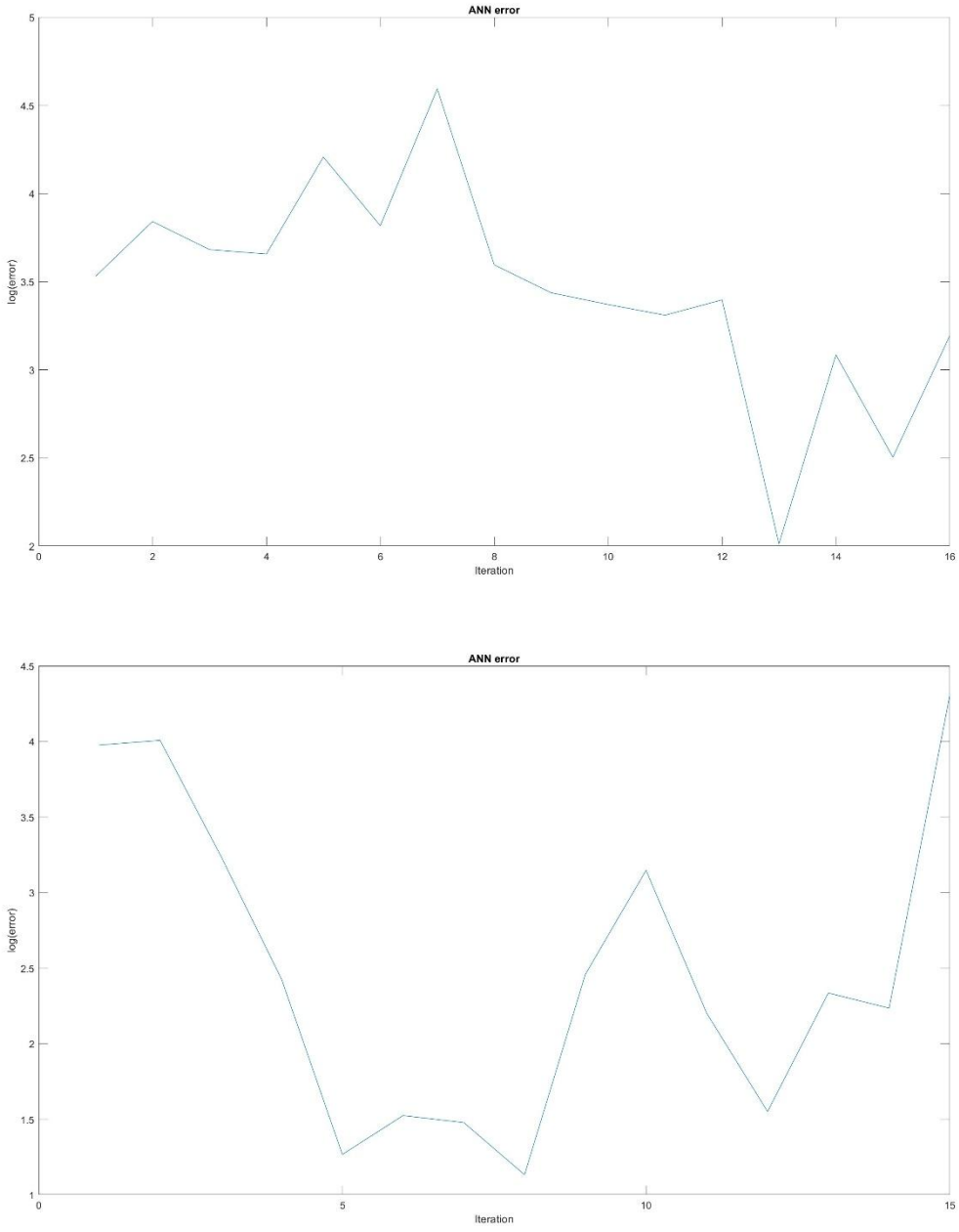

Figure 5.27 ANN error, Top: case 1, Bottom: case 2

5.5.4 Comparison of Genetics and NNO

The optimization process was carried out multiple times using the Genetic Algorithm (GA) to compare its performance with the Neural Network Optimization (NNO) approach. The results obtained from GA and NNO showed noticeable differences, both in terms of accuracy and computational efficiency. One of the most significant distinctions between the two methods was the time required for optimization. Specifically, the GA took approximately 1.5 times longer than the NNO to complete the optimization process when applied to a model with only six Bouc-Wen parameters.

This difference in computational efficiency became even more pronounced when attempting to scale the problem. While the NNO successfully handled an extended version of the model involving nine Bouc-Wen parameters, replicating the same optimization using GA proved impracticable. The system failed to complete the task due to the significantly higher computational load. This highlights a major limitation of GA in handling high-dimensional optimization problems compared to the more scalable and efficient NNO method.

Optimization variables which are the Bouc-Wen parameters, and their values are mentioned in Table 5.9.

Parameters	Results of GA
A	6.4096
β	0.6463
γ	0.4153
α	0.5011
D	0.9277
K0	0.6967

Table 5.9 Optimization variables and their values

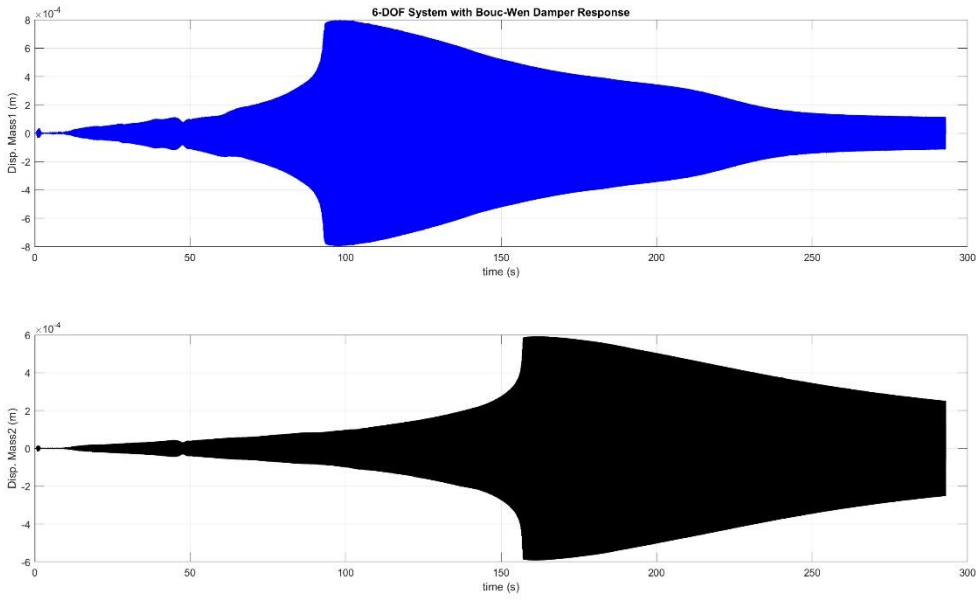

Figure 5.28 Displacements of the Stockbridge Dampers

As it is seen in Figure 5.29 although the displacements of the optimized data are close to the experimental ones, they lack the accuracy of the NNO in the previous section in Figure 5.16.

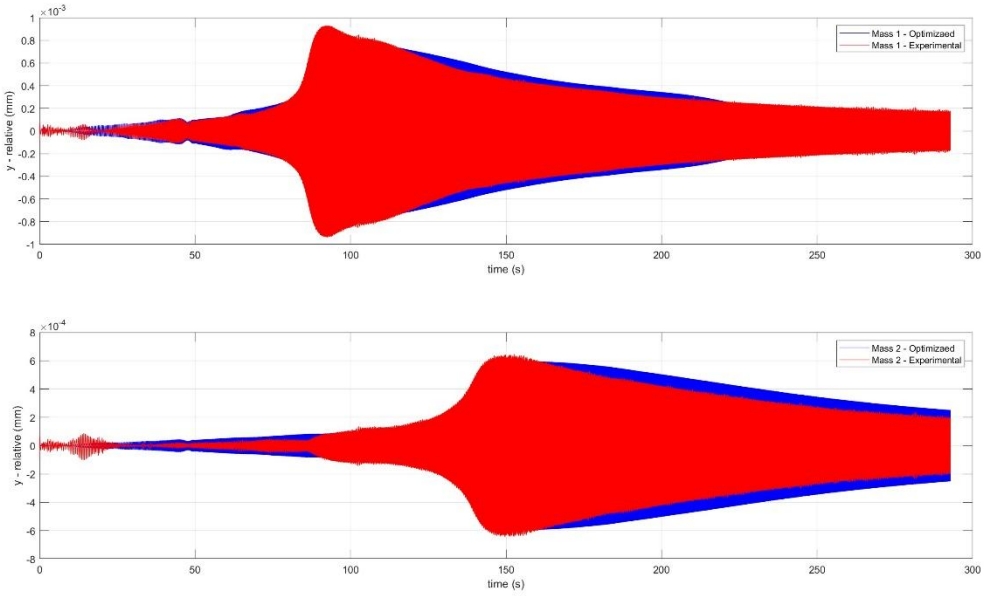

Figure 5.29 Comparison of the Displacements of the Experimental and Optimized data

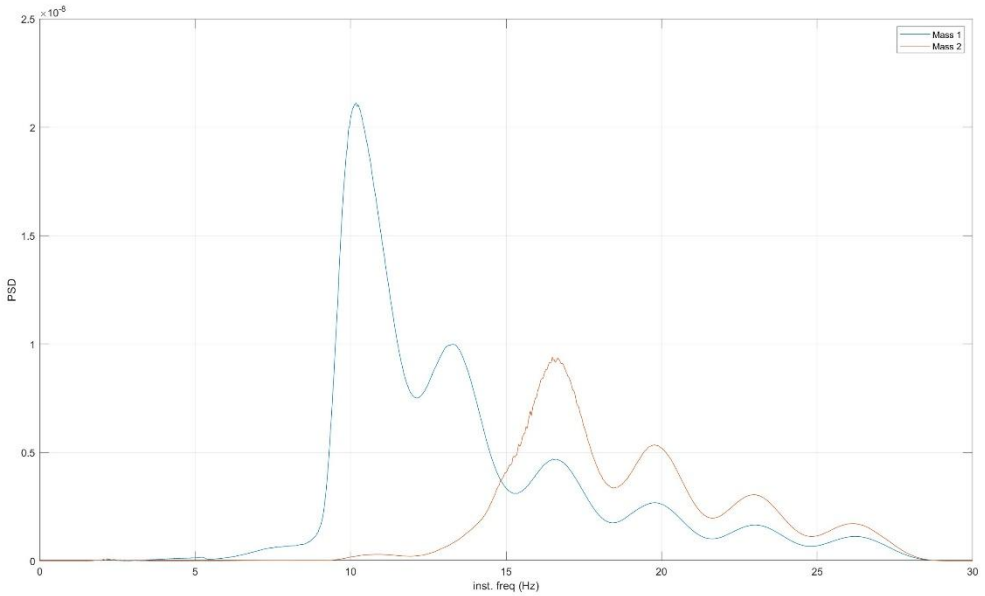

Figure 5.30 PSD of the optimized data

Figure 5.31 and Figure 5.33 show the comparison of experimental and optimized PSDs and shows the inaccuracy of the data. Figure 5.32 and Figure 5.34 show this comparison in a broader range and it is clear that they lack the accuracy of the NNO.

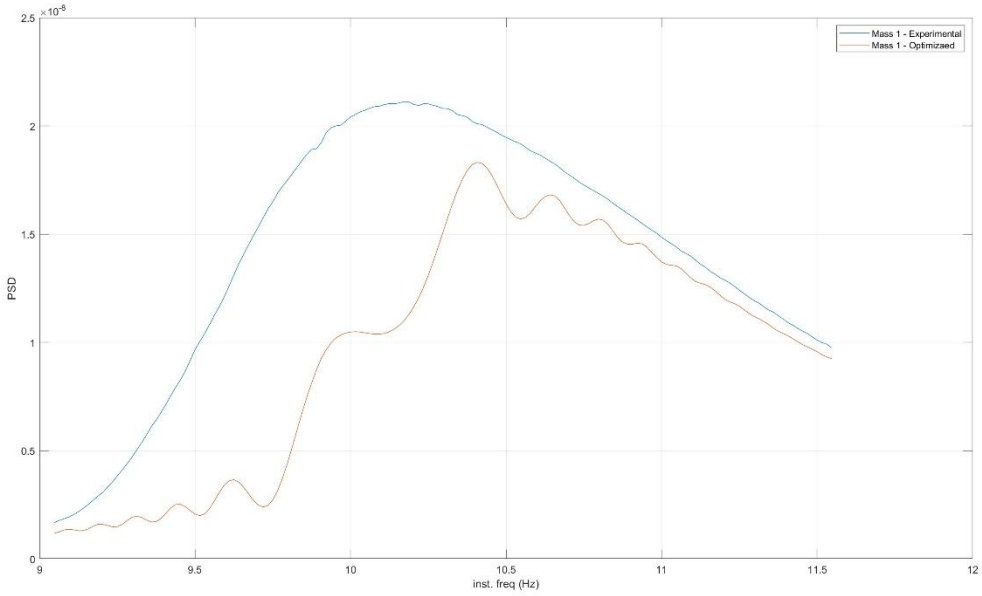

Figure 5.31 Peak of PSD of mass 1 in the range of 9 to 11.5 Hz

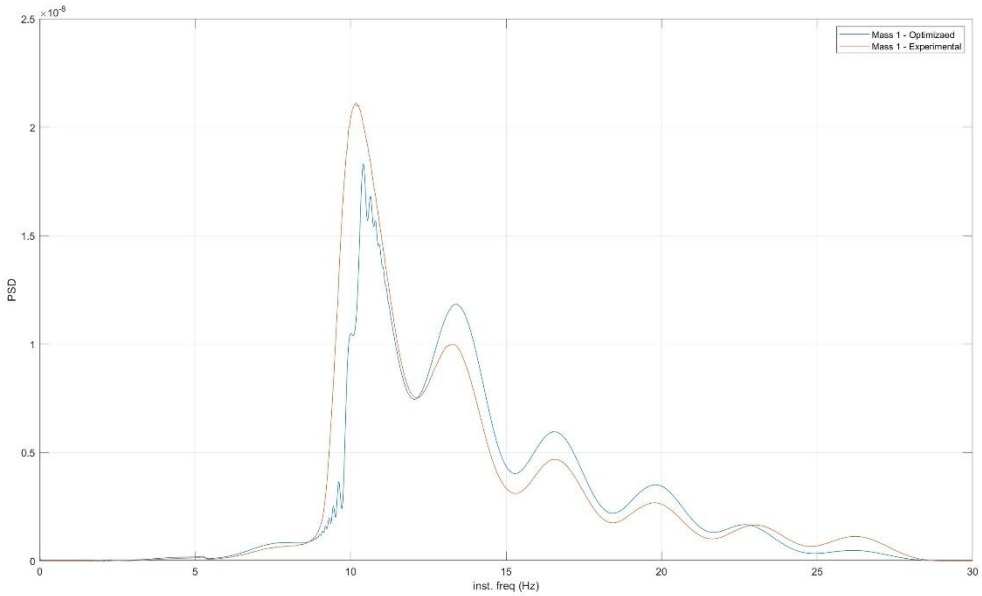

Figure 5.32 Experimental and optimized PSDs of mass 1

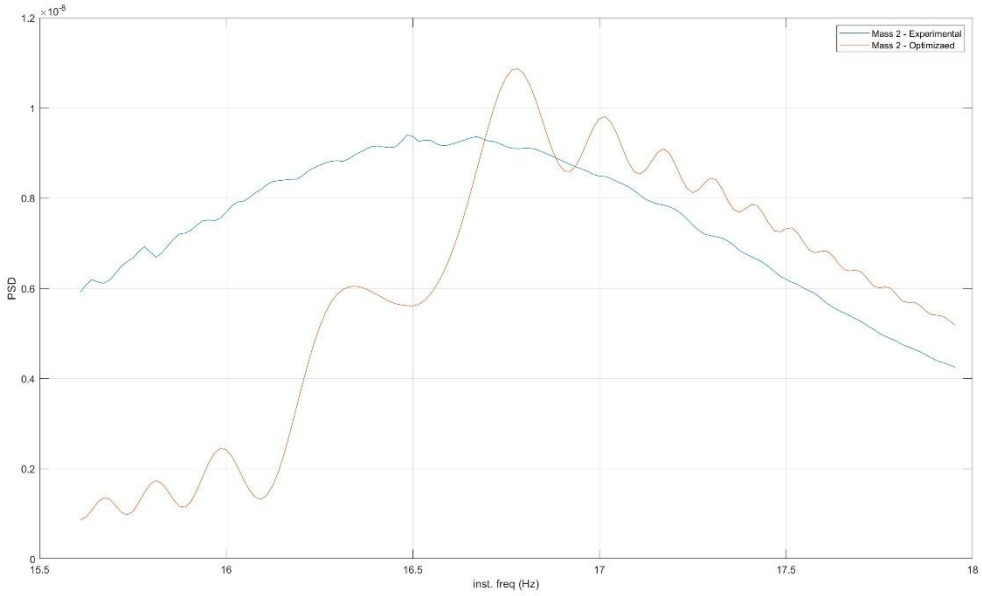

Figure 5.33 Peak of PSD of mass 2 in the range of 15.5 to 18 Hz

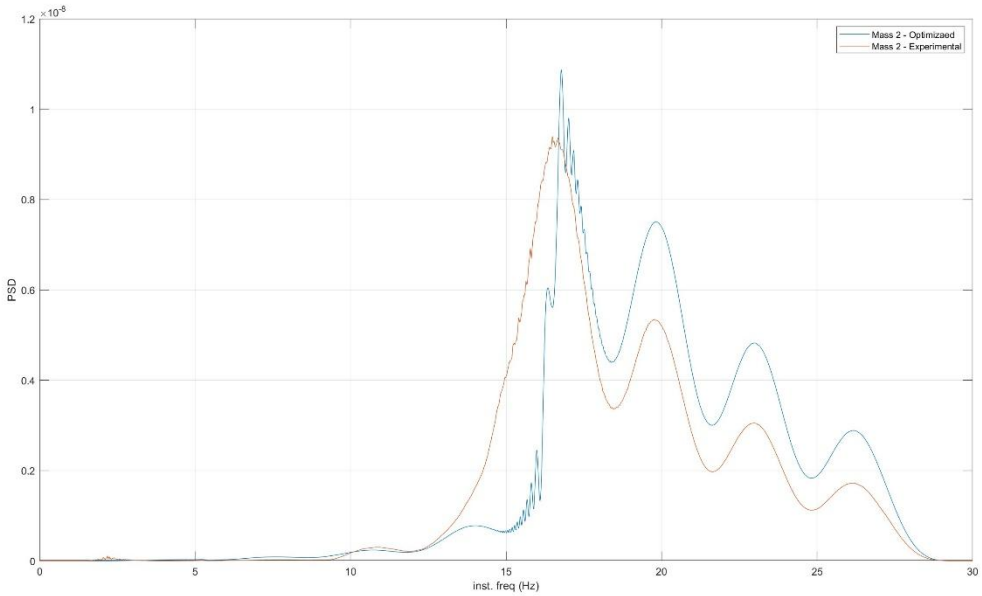

Figure 5.34 Experimental and optimized PSDs of mass 2

6 References

[1] H. Wagner, V. Ramamurti, R. V. R. Sastry, and K. Hartmann, “Dynamics of stockbridge dampers,” *Journal of Sound and Vibration*, vol. 30, no. 2, pp. 207-IN2, Sep. 1973, doi: 10.1016/S0022-460X(73)80114-2.

[2] O. Barry, J. W. Zu, and D. C. D. Oguamanam, “Nonlinear Dynamics of Stockbridge Dampers,” *Journal of Dynamic Systems, Measurement, and Control*, vol. 137, no. 061017, Jun. 2015, doi: 10.1115/1.4029526.

[3] O. Barry, D. C. Oguamanam, and D. C. Lin, “Aeolian vibration of a single conductor with a Stockbridge damper,” *Proceedings of the Institution of Mechanical Engineers, Part C: Journal of Mechanical Engineering Science*, vol. 227, no. 5, pp. 935–945, May 2013, doi: 10.1177/0954406212452064.

[4] Gilbert/Commonwealth (Firm), *Transmission Line Reference Book: Wind-induced Conductor Motion : Based on EPRI Research Project 792*. Electric Power Research Institute, 1979.

[5] F. Foti and L. Martinelli, “Hysteretic Behaviour of Stockbridge Dampers: Modelling and Parameter Identification,” *Mathematical Problems in Engineering*, vol. 2018, no. 1, p. 8925121, 2018, doi: 10.1155/2018/8925121.

[6] N. Barbieri and R. Barbieri, “Dynamic Analysis of Stockbridge Damper,” *Advances in Acoustics and Vibration*, vol. 2012, no. 1, p. 659398, 2012, doi: 10.1155/2012/659398.

[7] Q. Albu-Jasim and G. Papazafeiropoulos, “A Neural Network Inverse Optimization Procedure for Constitutive Parameter Identification and Failure Mode Estimation of Laterally Loaded Unreinforced Masonry Walls,” *CivilEng*, vol. 2, no. 4, Art. no. 4, Dec. 2021, doi: 10.3390/civileng2040051.

[8] “A review of the artificial neural network surrogate modeling in aerodynamic design - Gang Sun, Shuyue Wang, 2019.” Accessed: Jun. 16, 2025. [Online]. Available: https://journals.sagepub.com/doi/abs/10.1177/0954410019864485

[9] A. Dadras Eslamlou and S. Huang, “Artificial-Neural-Network-Based Surrogate Models for Structural Health Monitoring of Civil Structures: A Literature Review,” *Buildings*, vol. 12, no. 12, Art. no. 12, Dec. 2022, doi: 10.3390/buildings12122067.

[10] P. Ghafariasl *et al.*, “Neural network-based surrogate modeling and optimization of a multigeneration system,” *Applied Energy*, vol. 364, p. 123130, Jun. 2024, doi: 10.1016/j.apenergy.2024.123130.

[11] F. H. F. Leung, H. K. Lam, S. H. Ling, and P. K. S. Tam, “Tuning of the structure and parameters of a neural network using an improved genetic algorithm,” *IEEE Transactions on Neural Networks*, vol. 14, no. 1, pp. 79–88, Jan. 2003, doi: 10.1109/TNN.2002.804317.

[12] N. Barbieri, R. Barbieri, R. A. da Silva, M. J. Mannala, and L. de S. V. Barbieri, “Nonlinear dynamic analysis of wire-rope isolator and Stockbridge damper,” *Nonlinear Dyn*, vol. 86, no. 1, pp. 501–512, Oct. 2016, doi: 10.1007/s11071-016-2903-1.

[13] M. Kraus and P. Hagedorn, “Aeolian vibrations: wind energy input evaluated from measurements on an energized transmission line,” *IEEE Transactions on Power Delivery*, vol. 6, no. 3, pp. 1264–1270, Jul. 1991, doi: 10.1109/61.85875.

[14] M. L. Lu and J. K. Chan, “An Efficient Algorithm for Aeolian Vibration of Single Conductor With Multiple Dampers,” *IEEE Transactions on Power Delivery*, vol. 22, no. 3, pp. 1822–1829, Jul. 2007, doi: 10.1109/TPWRD.2007.899779.

[15] J. Vecchiarelli, I. G. Currie, and D. G. Havard, “COMPUTATIONAL ANALYSIS OF AEOLIAN CONDUCTOR VIBRATION WITH A STOCKBRIDGE-TYPE DAMPER,”

Journal of Fluids and Structures, vol. 14, no. 4, pp. 489–509, May 2000, doi: 10.1006/jfls.1999.0279.
[16] G. Diana, A. Cigada, M. Belloli, and M. Vanali, "Stockbridge-type damper effectiveness evaluation. I. Comparison between tests on span and on the shaker," *IEEE Transactions on Power Delivery*, vol. 18, no. 4, pp. 1462–1469, Oct. 2003, doi: 10.1109/TPWRD.2003.817797.
[17] S. Wiendl, P. Hagedorn, and D. Hochlenert, "Control of a test rig for vibration measurements of overhead transmission lines," in *2009 IEEE International Conference on Control and Automation*, Dec. 2009, pp. 2129–2135. doi: 10.1109/ICCA.2009.5410335.
[18] N. Barbieri and R. Barbieri, "Dynamic Analysis of Stockbridge Damper," *Advances in Acoustics and Vibration*, vol. 2012, no. 1, p. 659398, 2012, doi: 10.1155/2012/659398.
[19] O. Barry, J. W. Zu, and D. C. D. Oguamanam, "Forced Vibration of Overhead Transmission Line: Analytical and Experimental Investigation," *Journal of Vibration and Acoustics*, vol. 136, no. 041012, May 2014, doi: 10.1115/1.4027578.
[20] Cartmell MP, Ziegler SW, Khanin R., and D. Forehand, "Multiple scales analyses of the dynamics of weakly nonlinear mechanical systems," *Applied Mechanics Reviews*, vol. 56, no. 5, pp. 455–492, Aug. 2003, doi: 10.1115/1.1581884.
[21] E. Özkaya, "NON-LINEAR TRANSVERSE VIBRATIONS OF A SIMPLY SUPPORTED BEAM CARRYING CONCENTRATED MASSES," *Journal of Sound and Vibration*, vol. 257, no. 3, pp. 413–424, Oct. 2002, doi: 10.1006/jsvi.2002.5042.
[22] E. Özkaya, M. Pakdemirli, and H. R. Öz, "NON-LINEAR VIBRATIONS OF A BEAM-MASS SYSTEM UNDER DIFFERENT BOUNDARY CONDITIONS," *Journal of Sound and Vibration*, vol. 199, no. 4, pp. 679–696, Jan. 1997, doi: 10.1006/jsvi.1996.0663.
[23] E. Özkaya and M. Pakdemirli, "NON-LINEAR VIBRATIONS OF A BEAM–MASS SYSTEM WITH BOTH ENDS CLAMPED," *Journal of Sound and Vibration*, vol. 221, no. 3, pp. 491–503, Apr. 1999, doi: 10.1006/jsvi.1998.2003.
[24] M. Pakdemirli and A. H. Nayfeh, "Nonlinear Vibrations of a Beam-Spring-Mass System," *Journal of Vibration and Acoustics*, vol. 116, no. 4, pp. 433–439, Oct. 1994, doi: 10.1115/1.2930446.
[25] T. T. Baber and Y. K. Wen, "Stochastic Equivalent Linearization for Hysteretic, Degrading, Multistory Strutctures," *Civil Engineering Studies SRS-471*, Apr. 1980, Accessed: Jun. 16, 2025. [Online]. Available: https://hdl.handle.net/2142/14078
[26] F. Ikhouane, J. E. Hurtado, and J. Rodellar, "Variation of the hysteresis loop with the Bouc–Wen model parameters," *Nonlinear Dyn*, vol. 48, no. 4, pp. 361–380, Jun. 2007, doi: 10.1007/s11071-006-9091-3.
[27] C.-M. Chang, S. Strano, and M. Terzo, "Modelling of Hysteresis in Vibration Control Systems by means of the Bouc-Wen Model," *Shock and Vibration*, vol. 2016, no. 1, p. 3424191, 2016, doi: 10.1155/2016/3424191.
[28] J. P. Noël, A. F. Esfahani, G. Kerschen, and J. Schoukens, "A nonlinear state-space approach to hysteresis identification," *Mechanical Systems and Signal Processing*, vol. 84, pp. 171–184, Feb. 2017, doi: 10.1016/j.ymssp.2016.08.025.
[29] K. Challa, "Modelling and experimental characterization of Stockbridge dampers," laurea, Politecnico di Torino, 2023. Accessed: Jun. 16, 2025. [Online]. Available: https://webthesis.biblio.polito.it/29795/